



Piperazine-2-carboxylic acid derivatives as *MTDLs* anti-Alzheimer agents: Anticholinesterase activity, mechanistic aspect, and molecular modeling studies

Aya M. Soliman^a, Hend A.A. Abd El-wahab^a, Hulya Akincioglu^b, İlhami Gülçin^{c,*}, Farghaly A. Omar^{a,*}

^a Department of Medicinal Chemistry, Faculty of Pharmacy, Assiut University, 71526 Assiut, Egypt

^b Department of Chemistry, Faculty of Science and Arts, Agri-Ibrahim Cecen University, 04100 Agri, Turkey

^c Department of Chemistry, Faculty of Science, Ataturk University, 25240 Erzurum, Turkey

ARTICLE INFO

Keywords:

Piperazinylcarboxylic acids
Alzheimer's disease
Cholinesterase inhibitors
Cytotoxicity
Molecular modeling

ABSTRACT

Development of Multitarget-Directed Ligands (MTDLs) is a promising approach to combat the complex etiologies of Alzheimer's disease (AD). Herein we report the design, synthesis, and characterization of a new series of 1,4-bisbenzylpiperazine-2-carboxylic acid derivatives **3-5(a-g)**, **7a-f**, **8a-s**, and their piperazine-2-yl-1,3,4-oxadiazole analogs **6a-g**. *In vitro* inhibitory effect against *Electrophorus electricus* acetylcholinesterase (AChE) and butyrylcholinesterase (BChE) from *Equine* serum was evaluated using modified Ellman's method, considering donepezil and tacrine as reference drugs. Lineweaver–Burk plot analysis of the results proved competitive inhibition of AChE and BChE with K_i values, in low micromolar range. The free carboxylic acid series **4a-g** showed enhanced selectivity for AChE. Hence, **4c**, 1,4-bis (4-chlorobenzyl)-piperazinyl-2-carboxylic acid, was the most active member of this series (K_i (AChE) = $10.18 \pm 1.00 \mu\text{M}$) with clear selectivity for AChE ($SI \sim 17.90$). However, the hydroxamic acids **7a-f** and carboxamides **8a-s** congeners were more potent and selective inhibitors of BChE ($SI \sim 5.38 - 21862.5$). Extraordinarily, 1,4-bis (2-chlorobenzyl)-piperazinyl-2-hydroxamic acid **7b** showed promising inhibitory activity against BChE enzyme ($K_i = 1.6 \pm 0.08 \text{ nM}$, $SI = 21862.5$), that was significantly superior to that elicited by donepezil ($K_i = 12.5 \pm 2.6 \mu\text{M}$) and tacrine ($K_i = 17.3 \pm 2.3 \text{ nM}$). Cytotoxicity assessment of **4c** and **7b**, on human neuroblastoma (SH-SY5Y) cell lines, revealed lower toxicity than staurosporine and was nearly comparable to that of donepezil. Molecular docking and molecular dynamics simulation afforded unblemished insights into the structure–activity relationships for AChE and BChE inhibition. The results showed stable binding with fair H-bonding, hydrophobic and/or ionic interactions to the catalytic and peripheral anionic sites of the enzymes. *In silico* predicted ADME and physicochemical properties of conjugates showed good CNS bioavailability and safety parameters. In this regard, compound (**7b**) might be considered as a promising inhibitor of BChE with an innovative donepezil-based anti-Alzheimer activity. Further assessments of the most potent AChE and BChE inhibitors as potential *MTDLs* anti-Alzheimer's agents are under investigation with our research group and will be published later.

1. Introduction

Alzheimer's disease (AD) is a neurodegenerative disorder associated with decreased activity of the cholinergic system in the brain. Acetylcholinesterase inhibitors (AChEIs) represent one of the substantially evaluated strategies that successfully increase the concentration of acetylcholine (ACh) in the brain, resulting in enhancement of cholinergic transmission and thus increased cognitive function [1–3]. Four

AChEIs have been approved, e.g., tacrine, donepezil, rivastigmine, and galantamine, for the treatment of AD symptoms [4]. However, a major drawback of their widespread use as a general therapy showed undesirable side effects such as hepatotoxicity, which imposes severe dose limits. Identification of a drug that could prevent or delay the progression of neurodegenerative pathology without side effects is the goal for medicinal chemists.

Acetylcholinesterase (AChE, EC 3.1.1.7) and butyrylcholinesterase

* Corresponding authors.

E-mail addresses: igulcin@atauni.edu.tr (İ. Gülçin), farghalyomar@pharm.aun.edu (F.A. Omar).

<https://doi.org/10.1016/j.bioorg.2023.106916>

Received 5 July 2023; Received in revised form 10 October 2023; Accepted 11 October 2023

Available online 21 October 2023

0045-2068/© 2023 Elsevier Inc. All rights reserved.

(BChE, EC 3.1.1.8) are two forms of cholinesterases, belonging to the family of serine hydrolases. BChE is an enzyme closely related to AChE and serves as a cholinergic neurotransmission co-regulator that hydrolyzes ACh. Unequivocally, AChE and BChE, show variable levels during disease progression. Under normal physiological conditions, maximum cholinesterase activity is due to AChE. However, as the disease progresses, AChE activity decreases in specific brain regions. Meanwhile, BChE activity increases to compensate for some of the functions of AChE in cholinergic neurons [5,6]. Consequently, inhibitors of both enzymes might supply added therapeutic value [7,8]. AChE has received much attention owing to its dual functionality – the classic catalytic or cholinergic and the noncholinergic manifested in the central and peripheral nervous system [9]. Research on the noncholinergic role of AChE has strengthened its reputation in the neurodegeneration disorders associated with AD. This is primarily mediated by the peripheral anionic site (PAS) and involves aggregation with the amyloid- β peptide (A β) and promotes A β fibrillogenic by forming stable AChE-A β complexes [10,11]. Hence, ligands that inhibit AChE activity and A β aggregation may result in improving the quality of life for the affected patients. Accordingly, a promising approach based mainly on developing novel Multi-Target Directed Ligands (MTDLs), for tackling the complex pathophysiology of AD, has been established [12,13].

The current investigation presents a design strategy based on structural modulation of donepezil molecule to afford novel MTDLs. The expected new compounds involving 1,4-bisbenzylpiperazine core structure bearing carboxylic, hydroxamic acid functionalities or 1,3,4-oxadiazoles on C-2 of the piperazine nucleus (Fig. 1).

The benzylpiperazine moiety is involved in several *ChE*s as an adequate binding group for interaction with the PAS and CAS, of the enzyme [4,14–16]. Meanwhile, hybrid molecules involving aryl and/or heteroaryl carboxylic acid fragments were recently recognized as *MTDLs*, e.g., tacrine-ferulic acid hybrids [17], and thiazoline carboxylic acid derivatives [18]. Furthermore, interesting review articles have been published reporting various 5- and/or 6-membered heterocycles displaying promising inhibitory activity against AChE and BChE [19,20].

The proposed design strategy has been primarily verified through a flexible alignment study of the expected compounds with donepezil. Fig. 2 illustrates full alignment of the N-1-benzyl-2-carboxylate fragment with the indanone nucleus of donepezil. Moreover, it is expected that the second benzyl moiety would supply more π - π stacking and H- π interaction in the binding pocket of the targeted enzyme. Furthermore, it has been recently reported that linking heterocyclic functionalities, e.g. thiazole and/or oxadiazole, to piperazine or piperidine skeleton in some new chemical entities resulted in enhancement of the observed cholinesterase inhibitory effects and suppressing other etiological factors involved in AD, e.g., overproduction of A β oligopeptides, formation of

neurofibrillary tangles (NFTs), disruption of metals homeostasis and formation of reactive oxygen species (ROS) [21–23]. The electronic and/or physicochemical characteristics of the designed molecules will be tuned through the effect of the substituent on the benzyl moiety to acquire proper interactions with the respective targets [24].

Herein we reported the inhibitory effect of the synthesized 1,4-bisbenzylpiperazine-2-carboxylic acids/-2-oxadiazolyl derivatives against *Electrophorus electricus* acetylcholine-esterase (AChE) and butyrylcholinesterase (BChE) from *Equine* serum. Finally, several *in silico* studies will be performed to explore the binding modes and significant structural features for interactions with the amino acid residues of the respective enzyme's active site.

2. Results and discussion

2.1. Chemistry

The synthesis pathways of the designed 1,4-bisbenzylpiperazine-2-carboxylic acid derivatives, 3-5(a-g), 7a-f, and 8a-s, as well as the -2-(1,3,4-oxadiazole-5-thiones) 6a-g are outlined in Scheme 1. The synthesis of the targeted compounds 2a-g started by condensation of 1,2-diaminoethane with two equivalents of the respective aromatic aldehydes in methanol at room temperature according to the reported procedure [25]. Next step involved the reduction of the resulting diimines 1a-g by NaBH₄ in methanol at room temperature, affording the corresponding diamines 2a-g. Cyclization of the diamines with ethyl 2,3-dibromopropionate in refluxing toluene and in the presence of triethylamine, giving the corresponding piperazinyl-2-carboxylic acid esters 3a-g [26].

Derivatization of the carboxylic acid ester was achieved through application of several reactions. Explicitly, hydrazinolysis of the esters 3a-g in refluxing ethanol affords the corresponding hydrazides 5a-g. Afterwards, treatment of the latter with methanolic solution of KOH and CS₂ to get the respective 5-(1,4-dibenzylpiperazin-2-yl)-1,3,4-oxadiazole-2(3H)-thiones 6a-g. Synthesis of 1,4-bis-benzylpiperazinyl-2-carboxylic acids 4a-g was obtained by either of the following two procedures, the first through alkaline hydrolysis of the respective esters 3a-g and then acidification. The second procedure through treatment of the starting diamines 2a-g with 2,3-dibromopropionic acid, in refluxing toluene and in the presence of triethylamine, resulting in precipitation of the required piperazinyl-2-carboxylic acids 4a-g in good yields (75 – 90 %). Additional filtration, and recrystallization from proper solvents give the pure carboxylic acids 4a-g. The reaction of the respective carboxylic acids, 4a-g, with ethyl chloroformate at 0–5 °C, in the presence of triethylamine, affords the reactive mixed anhydrides. Treatment of the latter *in situ* with hydroxylamine hydrochloride or the proper amines

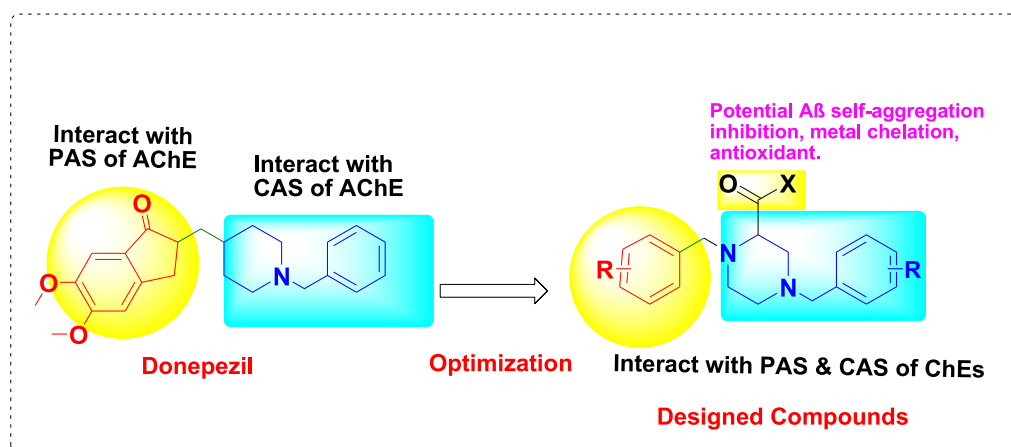


Fig. 1. Design strategy of the MTDLs: 1,4-bisbenzylpiperazine-2-carboxylic acid derivatives and the corresponding -2-(1,3,4-oxadiazole) analogs.

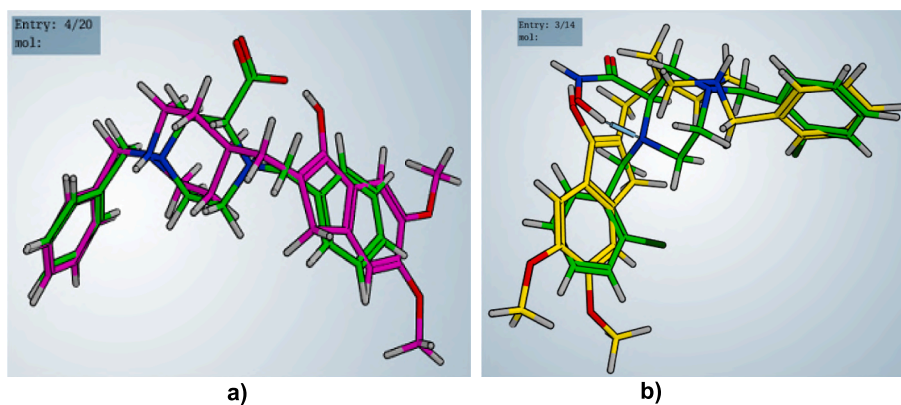
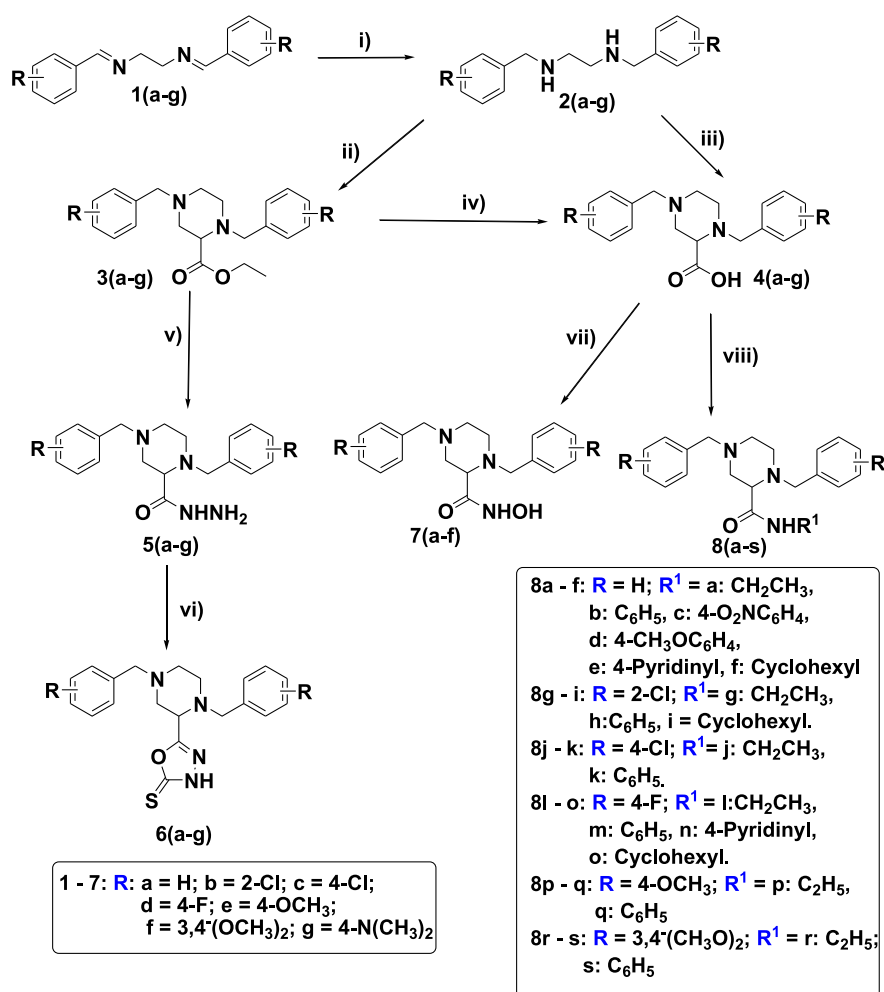


Fig. 2. a) Alignment of donepezil (purple) with 1,4-bisbenzylpiperazin-2-carboxylic acid (green). b) Donepezil (yellow) and the hydroxamic acid analog (green). (For interpretation of the references to color in this figure legend, the reader is referred to the web version of this article.)



Scheme 1. Reagents and conditions: i) NaBH₄, MeOH; ii) Ethyl 2,3-dibromopropionate, toluene, Et₃N, reflux; iii) 2,3-dibromopropionic acid, toluene, Et₃N, reflux; iv) NaOH, Dioxane, reflux. v) NH₂NH₂·H₂O, Ethanol, reflux; vi) CS₂, KOH, Methanol, reflux; vii) ClCOOC₂H₅, Et₃N, DCM, NH₂OH.HCl; viii) ClCOOC₂H₅, Et₃N, DCM, R¹NH₂.

affords the corresponding hydroxamic acids **7a-f** and the carboxamides **8a-s**, respectively.

IR, ¹H NMR, and ¹³C NMR spectra, as well as elemental analyses confirmed the structures of the synthesized compounds. The IR spectra reveal absorption bands characteristic for key function groups. The clear signals involve the carboxylic OH: ~ 3424; the amidic NH: ~ 3418;

hydrazide NH₂: ~ 3311 cm⁻¹, and C=O stretching vibrations at ~ 1730 – 1625 cm⁻¹. The IR spectra of the piperazinyl-2-(oxadiazole-2(3H)-thiones) **6a-g** show absorption bands at 1520–1495 cm⁻¹ of the (C=S) group. More bands were also found at 3430, 1592, and 1463 cm⁻¹, showing the (NH, C=N, and C–N) components of the oxadiazole nucleus, respectively.

The ^1H NMR spectra (SI: S1–S49) of the studied compounds show the signals of the piperazine ring protons as multiplets within the range of $\delta \sim 1.19$ – 4.17 ppm. The benzylic $-\text{CH}_2-$ protons are almost positioned at $\delta \sim 2.91$ – 4.60 ppm, as doublet with $J = 12.8$ – 14.8 Hz, characteristic for AA' coupling. This nonequivalence of these protons is due to the presence of a carboxylic group on C-2 of the piperazine nucleus, imparting an electronic and stereochemical environment. The aromatic protons of the phenyl rings and those of the attached substituents appeared at the expected chemical shifts and multiplicity. Moreover, the carboxylic proton in compounds **4a–g** is mostly undetectable due to rapid exchange with the solvent, d_6 -DMSO, otherwise, some spectra showed broad singlets at $\delta \sim 9.52$ – 9.96 ppm. Alternatively, variable signals are detected for the carboxylic acid derivatives at the respective δ -values (ppm) ~ 1.11 and 4.0 (**3a–g**, ester triplet/quartet of CH_2CH_3); 3.7 and 9.1 (**5a–g**, CONHNH_2); 7.4 and 9.5 (**7a–f**, CONHOH), and 7.3 (**8a–s**, CONHR_1). Meanwhile, the $(-\text{NH}-)$ singlets of 1,3,4-oxadiazole series **6a–g**, are

detectable at $\delta \sim 8.32$ – 14.46 ppm.

The principal signals in ^{13}C NMR spectra (SI: S1–S49) of the piperazinyl-2-carboxylic acid derivatives show signals for $\text{C}=\text{O}$ group at δ -values ranging from 172.92 to 167.13 ppm. The piperazine C-atoms are assigned to the signals at $\delta \sim 40.24$ – 60.25 ppm, and the benzylic α -C atoms showed signals at $\delta \sim 52.88$ – 66.63 ppm. Additionally, the signals of the aromatic C atoms and the attached substituents are detectable at specific chemical shifts. On the other hand, ^{13}C NMR spectra of 1,3,4-oxadiazole-2-thione series **6a–g** revealed two characteristic signals at $\delta \sim 177.78$ – 178.30 ppm showing ($\text{C}=\text{S}$) and at $\delta \sim 159.64$ – 163.06 ppm due to ($\text{C}=\text{N}$).

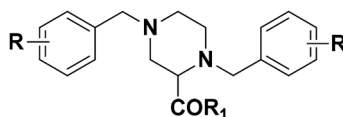
2.2. In vitro biological studies

2.2.1. Cholinesterase inhibitory activity

The *in vitro* inhibitory effect of the synthesized compounds, **4–6(a–g)**,

Table 1

Inhibition of cholinesterases by the studied MTDLs and the respective selectivity indices (SI) values.



Code	R	R ₁	AChE ^a		BChE ^a		SI ^b	
			Ki (μM)		Ki (μM)		AChE	BChE
4a	H	–OH	ND ^c		55.7 \pm 7.1			
4b	2-Cl		39.2 \pm 2.2		25.8 \pm 3.6		0.66	1.52
4c	4-Cl		10.2 \pm 1.0		182.2 \pm 25.4		17.90	0.06
4d	4-F		94.5 \pm 18.8		ND			
4e	4-OCH ₃		79.0 \pm 31.3		ND			
4f	3,4-(OCH ₃) ₂		30.7 \pm 5.1		120.8 \pm 72.7		3.93	0.25
5a	H	–NHNH ₂	ND		58.5 \pm 6.0			
5b	2-Cl		228.1 \pm 82.1		18.2 \pm 1.2		0.08	12.53
5c	4-Cl		50.6 \pm 3.2		101.7 \pm 44.0		2.01	0.49
6a	H		59.1 \pm 13.8		48.9 \pm 16.3		0.83	1.21
6b	2-Cl		56.0 \pm 2.2		10.4 \pm 3.0		0.19	5.67
6c	4-Cl		30.1 \pm 2.4		257.8 \pm 24.8		8.56	0.12
6e	4-OCH ₃		31.5 \pm 5.9		ND			
6f	3,4-(OCH ₃) ₂		111.8 \pm 60.2		45.9 \pm 13.6		0.41	2.44
6g	4-N(CH ₃) ₂		174.4 \pm 62.8		ND			
7a	H	–NHOH	ND		1.2 \pm 0.4			
7b	2-Cl		35.0 \pm 9.2		1.6 \pm 0.1*		0.00005	21862.5
7c	4-Cl		72.8 \pm 19.1		0.1 \pm 0.03		0.001	728.0
7d	4-F		ND		2.7 \pm 1.0			
7e	4-OCH ₃		26.0 \pm 7.7		0.9 \pm 0.4		0.03	28.88
7f	3,4-(OCH ₃) ₂		ND		420.1 \pm 149.8			
8a	H	–NHC ₂ H ₅	174.3 \pm 0.8		0.5 \pm 0.1		0.003	348.60
8b	H	–NHC ₆ H ₅	73.4 \pm 36.5		0.3 \pm 0.1		0.004	244.66
8c	H	–NH(4-O ₂ NC ₆ H ₄)	ND		1.2 \pm 0.4			
8d	H	–NH(4-OCH ₃ C ₆ H ₄)	98.2 \pm 12.3		1.4 \pm 0.4		0.01	70.14
8e	H	–NH (4-Pyridinyl)	50.5 \pm 11.2		5.2 \pm 1.8		0.10	9.71
8f	H	–NHC ₆ H ₁₁	18.2 \pm 6.8		0.9 \pm 0.1		0.049	20.22
8g	2-Cl	–NHC ₂ H ₅	ND		10.4 \pm 2.3			
8h	2-Cl	–NHC ₆ H ₅	ND		22.2 \pm 9.8			
8i	2-Cl	–NHC ₆ H ₁₁	44.5 \pm 5.3		0.8 \pm 0.4		0.02	56.62
8j	4-Cl	–NHC ₂ H ₅	ND		5.1 \pm 0.7			
8k	4-Cl	–NHC ₆ H ₅	ND		11.0 \pm 4.2			
8l	4-F	–NHC ₂ H ₅	ND		7.0 \pm 1.7			
8m	4-F	–NHC ₆ H ₅	56.3 \pm 28.3		8.6 \pm 1.7		0.15	5.54
8o	4-F	–NHC ₆ H ₁₁	ND		4.0 \pm 0.4			
8p	4-OCH ₃	–NHC ₂ H ₅	ND		7.1 \pm 1.1			
8q	4-OCH ₃	–NHC ₆ H ₅	ND		3.1 \pm 1.0			
8r	3,4-(OCH ₃) ₂	–NHC ₂ H ₅	69.3 \pm 7.7		12.9 \pm 0.8		0.19	5.38
8s	3,4-(OCH ₃) ₂	–NHC ₆ H ₅	ND		37.8 \pm 2.9			
Donepezil			0.7 \pm 0.1		12.5 \pm 2.6		17.85	0.07
Tacrine			1.2 \pm 0.1		17.4 \pm 2.3*		0.014	71.71

^aData is expressed as mean \pm standard error of mean (SEM), for three experiments.

^bSelectivity index (SI): $\text{AChE} = \text{Ki} (\text{BChE}) / \text{Ki} (\text{AChE})$; $\text{BChE} = \text{Ki} (\text{AChE}) / \text{Ki} (\text{BChE})$.

^cND (not determined): inhibitory potency lower than 50 % at 10 μM .

*These results are in nanomolar concentrations (nM).

7a-f, and **8a-s**, were evaluated against *Electrophorus electricus* acetylcholinesterase (EeAChE) and equine serum butyrylcholinesterase (BChE) by modified Ellman's method [27,28]. Donepezil and tacrine were used as reference drugs, respectively. Table 1 summarizes the inhibition constant (K_i) values and the corresponding selectivity indices (SI) against the targeted AChE and BChE. The K_i values illustrate an intrinsic thermodynamic quantity that is independent of the substrate (ligand) concentration but depends on the enzyme (target) and inhibitor. Thus, comparisons can be more readily made among different laboratories to characterize inhibitors. However, IC_{50} values depend on concentrations of the enzyme, the inhibitor, and substrate, along with other experimental conditions [29].

The study involved the synthesized series (**3–8**), which vary in the carboxylic functionality found on C-2 of the piperazine core nucleus. Explicitly, the esters **3a-g**; carboxylic acids **4a-g**; carbonylhydrazides **5a-g**; 1,3,4-oxadiazol-2-yl-5-thiones **6a-g**; hydroxamic acids **7a-f**; and carboxamides **8a-s**. The subclasses (**a-g**) or (**a-s**) are assigned to the respective type and pattern of substituents (R) attached to the benzyl moiety. The latter were selected to impart variable hydrophilic/lipophilic, electronic, and steric parameters, besides the possibility of affording extra binding as well as antioxidant characteristics. The results revealed that the tested compounds show *in vitro* inhibitory effect against AChE and BChE with K_i values in nanomolar to micromolar concentrations.

2.2.2. Kinetic study

In vitro inhibition study was carried out using modified Ellman's method to elucidate the mechanism of the observed inhibition of the studied compounds against EeAChE and equine serum BChE [27,28]. The K_i value is a dissociation constant that shows the binding affinity of an inhibitor against a specific enzyme. It can be derived from the Lineweaver-Burk graph obtained at three different inhibitor concentrations. The values are then calculated by taking the arithmetic average of three different independent values. The type of inhibition can be understood from the intersections on the x or y axes in the graphs. Broadly, there are three basic types of enzyme inhibition, including competitive, noncompetitive, and uncompetitive.

The Lineweaver-Burk reciprocal plots ($1/V$ vs $1/S$) (**SI: Kinetic study**) for each of the studied compounds revealed that all compounds have diverse slopes and intercepts on x-axis and the same intercept on the y-axis at increasing concentrations of the inhibitors. This pattern proves competitive inhibition of the investigated compounds on both AChE and BChE. Representative Lineweaver-Burk plots of **4c** and **7b** are illustrated in Fig. 3.

2.2.3. Cytotoxicity study

The safety of the most active inhibitors (**4c** and **7b**) was evaluated by investigating their cytotoxicity against human neuroblastoma (SH-SY5Y) cell lines, using 3-[4,5-dimethylthiazol-2-yl]-2,5-diphenyl tetrazolium bromide (MTT) assay method, [30,31], (**SI: Cytotoxicity**). The assay involves the formation of insoluble purple formazan crystals upon treatment of yellowish solutions of MTT dye with viable cells. The process depends on the ability of mitochondrial dehydrogenases of viable cells to cleave the tetrazolium ring.

The crystals were dissolved in acidified isopropanol and the resulting purple solution was measured spectrophotometrically. An increase or decrease in cell number results in a concomitant change for formazan formed, showing the degree of cytotoxicity caused by the test material. Compounds **4c** and **7b**, exhibit lower cytotoxicity, (Table 2), on neuroblastoma cell lines compared to that of the reference drug, Staurosporine; however, they displayed relatively higher cytotoxicity than donepezil.

2.3. Structure activity relationship (SAR) analysis

As previously said in the design strategy, the current investigation is based on structural modulation of donepezil molecule to afford novel MTDLs. The structural modifications aimed at keeping the essential pharmacophoric features of the lead drug, viz. H-bonding, hydrophobic interactions, as well as π - π or π -H stacking with the target enzyme. Primarily, the postulated strategy was proved through a flexible alignment study, as illustrated in Fig. 2. The investigated compounds entailing 1,4-bisbenzyl-piperazine core structure loaded with carboxylic, hydroxamic acid, carboxamide functionalities or 1,3,4-oxadiazole as rigid cyclized isosteric analogs on C-2.

Analysis of the observed inhibitory effects (Table 1) against cholinesterases demonstrates some interesting SAR attributes (Fig. 4). The ester series **3a-g** showed inhibitory potency lower than 50 % at a concentration of 10 μ M and are not considered in the study. This series is lipophilic prodrugs of the corresponding acids, **4a-f**, by masking the

Table 2

The results of cytotoxicity study of **4c** and **7b** on SH-SY5Y cell lines.

Compounds	IC_{50} (μ M)
4c	55.26 \pm 2.48
7b	37.46 \pm 1.68
Donepezil	87.26 \pm 3.92
Staurosporine	21.57 \pm 0.97

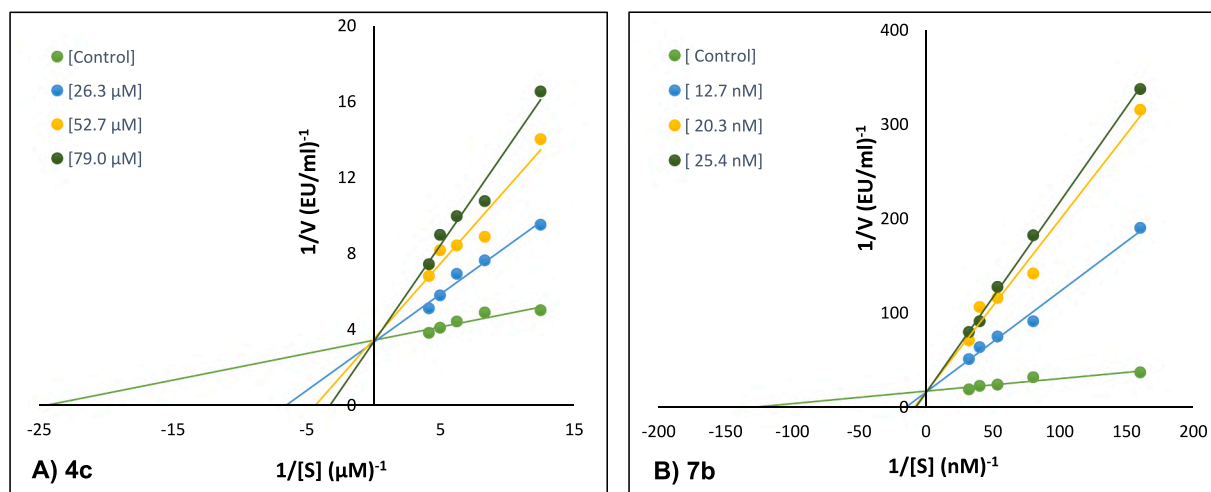


Fig. 3. Lineweaver-Burk plot for inhibition of AChE (A) and BChE (B) by compounds **4c** and **7b**, respectively.

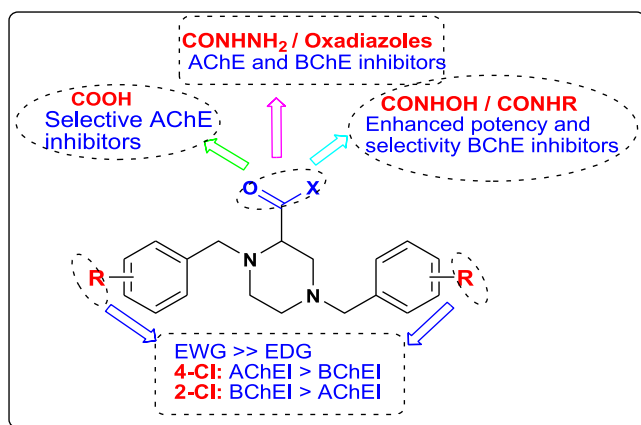


Fig 4. Diagrammatic representation of SAR attributes of the studied donepezil-based 1,4-bisbenzylpiperazine-2-carboxylic acid derivatives.

polar carboxylic acid functionalities. This might imply enhanced probability for crossing the blood–brain barrier (BBB) *in vivo*. Hydrolysis inside the brain by esterase enzymes affords high concentrations of the active compounds. Assessment of this aspect is scheduled for future investigations.

Unequivocally, the carboxylic acid series **4a–f** showed selective inhibitory activity against AChE, with K_i values in the range of $(10.2 \pm 1.0–94.5 \pm 18.8 \mu\text{M})$. However, the corresponding K_i values of carboxylic acid derivatives **4(a, b, c, f)** against BChE are in the range of $25.8 \pm 3.6–182.2 \pm 25.4 \mu\text{M}$. The most potent member within this series against AChE is the 4-chlorobenzyl derivative **4c** ($K_i = 10.2 \pm 1.0 \mu\text{M}$, $SI = 17.9$); vs. its 2-chloro analog **4b**, showing comparable inhibition of BChE ($K_i = 25.8 \pm 3.6 \mu\text{M}$). Modification of the parent acids **4a–g** to the carbohydrazides, **5a–g** results generally in decreased inhibitory activity against both enzymes. The carbohydrazide **5b** with 2-chloro-benzyl substituent is the most potent derivative within this series (K_i (BChE) = $18.2 \pm 1.2 \mu\text{M}$) exceeding its 4-chloro congener, **5c** (K_i (AChE) = $50.6 \pm 3.12 \mu\text{M}$). Further, modification of the hydrazides **5a–g** to the corresponding -2-(1,3,4-oxadiazol-2-yl-5-thiones) **6a–g** keeps similar pattern with enhanced inhibitory activity against BChE and AChE, as showed by compounds **6b** and **6c** ($K_i = 10.4 \pm 3.0$ and $30.1 \pm 2.4 \mu\text{M}$, respectively).

The results of inhibition of cholinesterases elicited by the piperazinyl-2-hydroxamic acid series **7a–f** and the amides **8a–s**, (Table 1), show substantial selectivity for BChE. Principally, 1,4-bis(2-chlorobenzyl)-piperazine-2-hydroxamic acid **7b** displayed nanomolar inhibitory activity against BChE ($K_i = 1.6 \pm 0.1 \text{ nM}$; $SI = 21862.5$) being supreme potency of the studied compounds. Its K_i value exceeds enormously that of the reference drugs, donepezil and tacrine ($K_i = 12.5 \pm 2.6 \mu\text{M}$ & $17.3 \pm 2.3 \text{ nM}$, respectively). A similar pattern of inhibition has been seen for congeners **7(a, c, d, and e)**, displaying inhibition of BChE at single digit to sub-micromolar concentrations (K_i values = 1.2 ± 0.4 , 0.1 ± 0.03 , 2.7 ± 1.0 , and $0.9 \pm 0.4 \mu\text{M}$, respectively). Likewise, the inhibitory profiles of the amide series **8a–s** revealed selective inhibition of BChE. The results show a promising range of K_i values $\sim 0.3 \pm 0.1–37.8 \pm 2.9 \mu\text{M}$. Meanwhile, the observed inhibitory activities of this series against AChE are limited. Only 9 compounds out of 19 exhibit inhibitory effects, with K_i values ranging in $18.2 \pm 6.8–174.2 \pm 0.9 \mu\text{M}$. Interestingly, similar inhibitory patterns were recently reported for a series of imino-2H-chromene carboxamides demonstrating 10-folds selectivity for BChE vs. AChE [32].

Concerning the substituents (**R**) in the benzyl moieties, the results reveal that the presence of EWGs enhances the inhibitory activity compared to the EDGs. As previously said in this section, 2-Cl and/or 4-Cl-substituted compounds prove superior inhibitory vs. 4-OCH₃ substituent. Nonetheless, the inhibitory activity of the 4-fluorobenzyl

derivatives **4d** and **7d**, (K_i (AChE) = 94.5 ± 18.8 and K_i (BChE) = $2.7 \pm 1.0 \mu\text{M}$, respectively), illustrating higher inhibitory concentrations (Low potency) than that of the chloro substituted analogs **4c** and **7c** (K_i (AChE) = 10.2 ± 1.0 and K_i (BChE) = $0.11 \pm 0.03 \mu\text{M}$, respectively). This might indicate that perfect orientation and interaction within the active site requires a specific bulkiness of the substituents attached to the benzyl moiety. However, this is not the case with the 4-fluorobenzyl carboxamides, e.g., **8l**, **m**, and **8o** (Table 1). These compounds show enhanced inhibitory effects against BChE ($K_i = 7.0 \pm 1.7$, 8.6 ± 1.7 , and $4.0 \pm 0.4 \mu\text{M}$, respectively). Thereby, the bulkiness of amide substituents groups compensates for the required orientation into the binding site of the enzyme.

A substantial SAR feature reflecting the impact of the position of the chloro substituent on the benzyl moiety is also obvious. Unlike, the 4-chlorobenzyl substituted compounds **4–6(c)**, that prove AChE selectivity ($SI = 2.01–17.90$), the 2-chlorobenzyl derivatives, **4–7(b)**, as well as **8i**, show selective inhibitory effects against BChE, ($SI = 1.52–21862.5$). The implication of the position of substituents found on the benzyl fragment attached to N4 of the piperazine nucleus has been previously reported. A study involving amiridine-piperazine hybrids shows that compounds with a *para*-substituted aromatic ring on N4 of the piperazine fragment displayed enhanced inhibition against AChE [33]. On the other hand, in a series of aryl-9-phosphoryl-9,10-dihydroacridines, the inhibitory activity against BChE was reduced tenfold, as the *para*-substituent is Cl, compared to the unsubstituted compound [34]. Similar pattern seen in our study, as the K_i (BChE) of the 4-chlorobenzyl derivative **4c** = $182.2 \pm 25.4 \mu\text{M}$, while the unsubstituted **4a** is more potent ($K_i = 55.7 \pm 7.1 \mu\text{M}$).

2.4. Molecular modeling studies

2.4.1. Molecular docking

Docking studies of the synthesized 1,4-bisbenzylpiperazine-2-carboxylic acid derivatives, using Molecular Operating Environment software (MOE 2020.01), were conducted to explore the structural basis of the observed differences in inhibitory activity. The target proteins were X-ray crystallographic structures of recombinant human AChE in complex with donepezil (PDB code: 4EY7) and that of BChE co-crystallized with tacrine (PDB code: 4BDS) [35–37].

Docking to the crystallographic structures of *Ee*AChE and Equine serum (BChE), that are used in enzyme inhibition assay was excluded. There is no ligand-enzyme complex reported for *Ee*AChE, so docking results will not be dependable and will require cross-validation using alternative software. Meanwhile, *Kuca, et al.* reported computational alignment showing higher degree of structural and functional conservation of AChEs from distinct species. The most significant difference involves mutations of Asp74 and Tyr124 in humans to Tyr71 and Met153 in *Drosophila*, respectively. This alters both the steric and electrostatic properties of the upper part of the active site gorge [38].

The active sites of hAChE and hBChE (SI: Fig. 50A, B), show a larger gorge of BChE than that of AChE (500 \AA^3 versus 300 \AA^3). Seems like a bowl rather than a deep, narrow gorge and has about 40 % fewer aromatic amino acid residues than AChE. Alternatively, smaller aliphatic or even polar residues are perceptible [39]. The 3D crystallographic structures (SI: Fig. 51A, B) and the respective ligand interactions diagrams (SI: Fig. 52A, B) of the selected hAChE and hBChE, co-crystallized with Donepezil (PDB code 4EY7) and tacrine (PDB code: 4BDS) respectively, are illustrated in the assigned supplementary material.

The docking algorithm was initially validated by redocking the native ligands, donepezil and tacrine into the active sites of target proteins. Ideally, a computational method's validity is appropriate when the root mean square deviation (RMSD) value is less than 2.0 \AA [40]. The respective validation criteria in this study showed $\text{rmsd} = 0.8343 \text{ \AA}$. Consequently, docking procedures were performed for the studied compounds **4–6(a–g)**, and **7a–f**. The results, compressing docking scores,

binding modes, and 2D ligand interactions diagrams are listed (SI: Tables S1 and S2). Analysis of the results revealed common features, showing comparable interactions and orientation patterns to those of the co-crystallized ligands. Obviously, the phenyl ring of the pendant benzyl substituents demonstrates π - π stacking interaction with Trp86 viz. Trp82, Trp286 and/or Tyr341. The carboxylate functionality on C-2 of the piperazine ring, and N-1-benzyl moiety acquire a binding pattern and orientation analogous to that of the indanone moiety of donepezil, within the PAS site. Interestingly, the interactions involve direct and/or H₂O-mediated H-bonding to the amino acid residues of the catalytic triad (Ser198, His438, Glu197). Representative examples are compounds **4b**, **4c**, and **7b**. However, the carboxamides **8a-s** showed an inverted orientation, whereby the distal benzyl moiety oriented towards the PAS. Remarkably, the designed compounds show extra binding interactions with more amino acids involving H-bonding, π -cation, and π - π stacking. These extra interactions played a substantial role in stabilizing ligands-target complexes. This might account for the apparent enhanced binding scores of the studied compounds vs. Donepezil and/or tacrine.

Alternatively, the docking scores, binding interactions, and the respective K_i values of the most active compounds within the studied classes **4-8**, are summarized in Table 3. The results show that the binding scores went in line with the K_i values. Apparently, compounds **4c**, **5c**, and **7e** with the lowest K_i values against AChE: 10.2 ± 1.0 , 50.6 ± 5.1 , and $26.0 \pm 7.7 \mu\text{M}$, demonstrated lower binding energy than donepezil to AChE: -18.51 , -20.19 , and -20.12 kcal/mol, respectively. Meanwhile, K_i value of compounds **7b**, **8a**, **8b**, and **8f** against BChE: 1.6

Table 3

Binding scores (Kcal/mol) and amino acid residues involved in H-bonding and hydrophobic interactions of the most active compounds.

Code	Enz.	Score	Interacting amino acids H-Bond	Hydroph. interactions	K_i (μM)
Don.	AChE	-17.50	Asp74(H ₂ O), His447, Arg296(H ₂ O), Phe295	Tyr341, Tyr337, Trp86, Tyr337	$0.7 \pm$ 0.1
Tac.	BChE	-8.74	Asp70(H ₂ O), Ser79, Thr120, His438	Trp82, Glu197	$17.4 \pm$ 2.3^*
4c	AChE	-18.51	Tyr124(H ₂ O),	Tyr341, Phe338,	$10.2 \pm$
	BChE	-8.28	Tyr133 Ser198, Pro285, His438	Tyr337, His447, Trp86 Trp231, Tyr332, Leu286	1.0 182.2 ± 25.4
5b	BChE	-8.85	Glu197, His438, Ser198, Asp70, Phe398	Trp82, Gly117, Leu286, Phe329	$18.2 \pm$ 1.2
5c	AChE	-20.19	Asp74(H ₂ O), Tyr133, Tyr124 (H ₂ O)	Tyr341, Phe338, Phe295, Phe297, Trp86	$50.6 \pm$ 3.2
6b	BChE	-9.00	His438, Ser198, Gly115, Phe398	Trp231, Trp82	$10.4 \pm$ 3.0
7b	AChE	-18.11	Ser125(H ₂ O),	Phe338, Tyr337,	$35.0 \pm$
	BChE	-11.17	Tyr124 (H ₂ O), Asp74 (H ₂ O), Phe295 Asp74(H ₂ O) Glu197, Gly116, Ser198, His438	Tyr341, Trp86, Trp82, Gly117, Trp82, Gly117, Leu286, Phe 329	9.2 $1.6 \pm$ 0.1^*
7e	AChE	-20.12	Tyr341, Val294, Tyr341	Trp286, Phe338, Tyr337 Tyr341	$26.0 \pm$ 7.7
8a	BChE	-9.04	Gly78, Gly116, Glu197, His438	Leu286, Trp231, His438	$0.5 \pm$ 0.1
8b	BChE	-9.39	His438(H ₂ O), Ser198, Thr120(H ₂ O)	His438, Trp430, Ala328, Phe329, Trp82	$0.3 \pm$ 0.1
8f	BChE	-9.22	Gly78, His438	Trp 82, Phe329, Trp 231	$0.9 \pm$ 0.1

Don. Donepezil; Tac. Tacrine.

*These results are in nanomolar concentrations (nM).

± 0.08 nM, 0.5 ± 0.1 , 0.3 ± 0.09 and $0.9 \pm 0.1 \mu\text{M}$ are correlated to their binding affinities: -11.17 , -9.04 , -9.39 and -9.22 kcal/mol, respectively.

As previously discussed, the respective amino acids in the active sites of AChE and BChE rationalize the disparity in the variable modes of interaction of the studied compounds. Compound **4c**, showed *in vitro* selectivity for AChE ($SI = 17.90$); meanwhile, its docking pose demonstrates perfect alignment with the co-crystallized donepezil, (Fig. 5A). The interactions involve: H-bonding of the protonated N1 of piperazine nucleus with Tyr124 through H₂O molecules and the 4-chloro substituent of the benzyl fragment to Tyr133, (SI: Table S1). In addition, there are π -H interactions of the C-atoms of piperazine ring, and methylene groups of the distal benzyl moiety with Tyr341, Phe338, Tyr337, His447, and Trp86. As reported by Richardson, *et al.* the two amino acids (Tyr124 and Tyr133) are part of a narrow bottleneck of gorge in AChE [34]. Consequently, these interactions might contribute to enhanced inhibitory activity against AChE. Meanwhile, the 3D representation of the docking pose of 2-chlorobenzyl-piperazine-2-hydroxamic acid, **7b** in the active site of AChE (Fig. 5B), reveals different binding modes. The latter involves direct H-bonding of the hydroxamic acid moiety to Phe295, water-mediated with Ser125, Tyr124, and Asp 74. Hydrophobic π -H interactions to Trp82, Gly117, Leu286, and Phe 329 were also perceptible.

On the other hand, docking of compound **4c** in the active site of BChE revealed a changed binding and orientation than the co-crystallized tacrine molecule (Fig. 6A). The docking pose shows interactions involving H-bonding of the 4-Cl substituent and C-3 of the piperazine ring with Ser198, Pro285, and His438. In addition, one phenyl groups form π -H interactions with Trp231 and Leu286, while the other phenyl showed π -H with Tyr332 with low binding affinity -8.28 Kcal/mol (SI: Table S2). Alternatively, the interactions of compound **7b**, (Fig. 6B), illustrate interactions involving direct H-bonding between OH of the hydroxamic acid moiety and Glu197 in the CAS. Additionally, 3H-bonding interactions were also seen between C-3 of the piperazine ring, the 2-Cl substituent with His438, Gly116, and Ser198, respectively. The distal 2-chlorophenyl moiety extends inside the larger gorge. Thereby, showing π -H interactions with Trp82, Gly117, Leu286 and Phe329. Interestingly, the hydrophobic interaction with Trp82 stands for a common feature (Table 3) for tacrine as well as the compounds eliciting selective inhibition against BChE. This amino acid residue is found deeper in the gorge than Asp70 and Tyr332 and forms the active site as a part of the cation-binding compartment [34].

2.4.2. Molecular dynamic simulations

Molecular dynamic simulation was assumed to confirm the binding poses of the most potent inhibitors, **4c** and **7b**, inside the active sites of the target enzymes. The molecular complexes of the two enzymes **4c** and **7b**, obtained from docking results, were subjected to 50-ns-long molecular dynamic simulations (MDS), using NAMD 3.0.0. software [41,42]. Protein systems were built using the QwikMD toolkit of the VMD software [43]. As shown in Fig. 7, both compounds showed good stability inside the respective active site over the course of simulation with an average RMSD values of 2.4 \AA and 1.8 \AA , respectively.

These binding stabilities, expressed as steady RMSDs profile, were comparable to that of the native inhibitors, donepezil, and tacrine (average RMSD = 1.4 \AA and 2.3 \AA). Moreover, the total electrostatic and van der Waals interactions energies averaged around -47.12 and -53.93 of **4c** and **7b** affording further evidence for the observed binding stability (Supporting information Fig. S55).

These results match the binding modes discussed in the earlier subsection. For ligand **4c**, H-bonding of the carboxylate moiety with Tyr133 and the 4-Cl substituent with Phe338 contribute profoundly to the observed stability inside the active site of hAChE. Meanwhile, ligand **7b** complex with hBChE is stabilized through H-bonding with Ser198 and His438 in the CAS of the enzyme. Additionally, their calculated binding

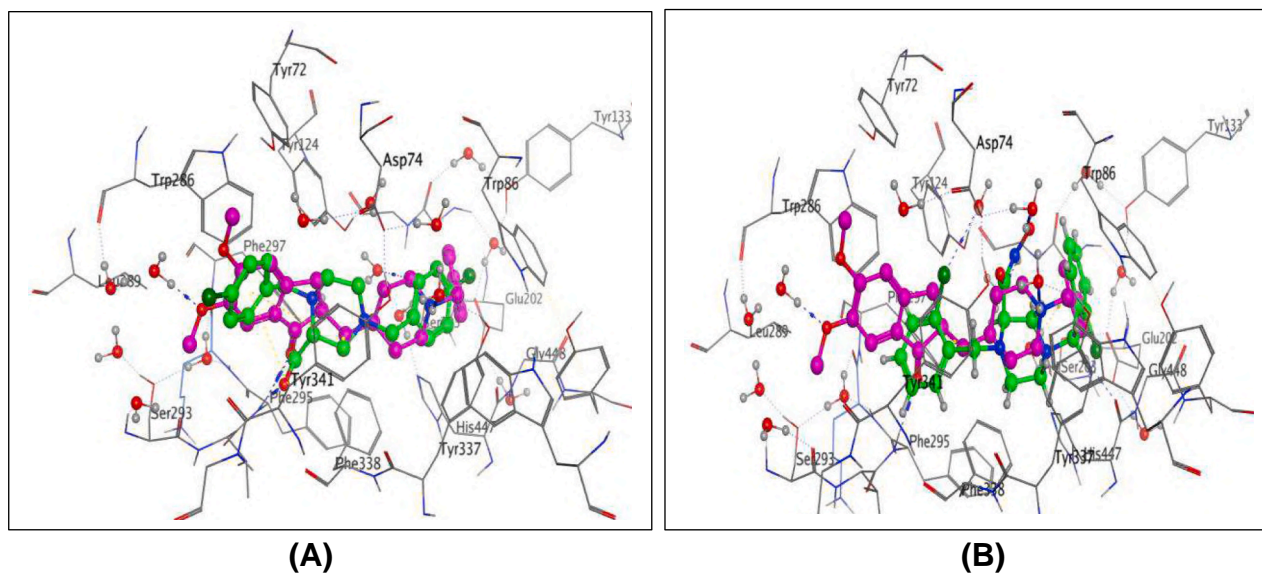


Fig. 5. A: 3D representation of **4c** (green), and **B:** **7b** (green) into the active site of hAChE (PDB ID: 4EY7); showing the co-crystallized ligand donepezil (purple). (For interpretation of the references to color in this figure legend, the reader is referred to the web version of this article.)

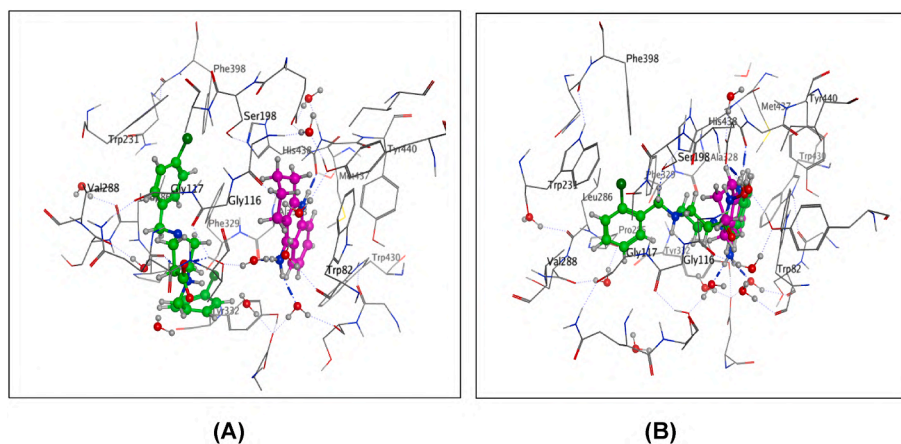


Fig. 6. A: 3D representation of **4c** (green), and **B:** **7b** (green) into the active site of hBChE (PDB ID: 4BDS), showing the co-crystallized ligand tacrine (purple). (For interpretation of the references to color in this figure legend, the reader is referred to the web version of this article.)

total free energies regarding MM-PBSA [44], were -13.11 and -12.49 kcal/mol, respectively, showing good affinities towards the corresponding active sites that were also comparable to that of donepezil and tacrine (Table 4). Both compounds proven stable multiple hydrophilic and hydrophobic interactions, particularly H-bonds that were around 2H-bonds throughout the simulation course (SI: Fig. S56). In conclusion, the achieved 50-ns MD simulation of compounds **4c** and **7b** showed good binding stability in the active sites of both AChE and BChE. Further comprehensive MD experiments, involving the two ligands, but on reversed order of the enzymes might afford conclusive evidence about their selectivity.

2.4.3. Molecular electrostatic potential (MEP) calculations

Molecular electrostatic potential (MEP) maps are related to total electron density and define regions of local negative and positive potential in a molecule.

They are often used to recognize regions susceptible to electrophilic and nucleophilic reactions, as well as hydrogen bonding interactions. In the electrostatic potential contour map, the negative regions (assigned to red) of MEP are related to electrophilic attacks, and positive regions (assigned to blue) are related to nucleophilic reactivity [45,46]. The

MEP diagrams of the hits **4c** and **7b** were visualized using MOE software. Unlike the computational methods, this software calculates and visualizes the MEP representations for the ligand molecules and the target protein. This will clearly demonstrate the possible complementarity, which might account for the observed interactions. Fig. 8 shows the presence of an electron-rich zone concentrated over the carboxylic oxygen atoms, indicating sites for electrophilic attack. Electrons in this region could be easily given to acceptor species. However, the most positive regions are around hydrogens bonded to nitrogen atoms, which makes these groups hydrogen bond donors. The electrostatic potential maps are clearly matched with the observed ligand-enzymes interactions as obvious in the 2D figures and binding modes (SI: Table S4).

2.4.4. Molecular characteristics and drug-likeness

Molecular characteristics are a complex balance of various structural features that generally determine the relevance of a particular molecule to known drugs. Hydrophobicity, molecular size, flexibility, and the presence of various pharmacophoric features are the main physico-chemical properties that influence the behavior of molecules in a living organism. Good bioavailability can be achieved with a proper balance between solubility and partitioning properties. Hence, compliance of the

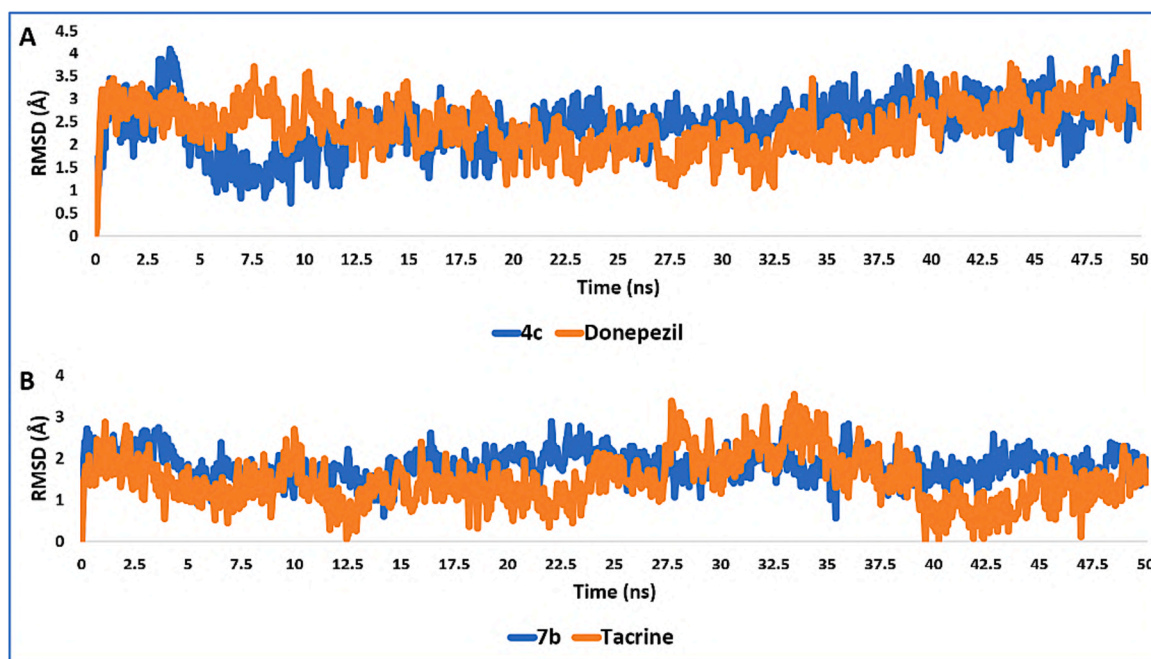


Fig. 7. (A) Evolution along MD trajectories of RMSD values for compounds **4c** and donepezil in the active site of hAChE; and (B) for compound **7b**, tacrine in the active site of hBChE.

Table 4

Binding free energies (MM-PBSA) of compounds **4c** and **7b** along with the native inhibitors in complex with AChE (PDB ID: 4EY7) and BChE (PDB ID: 4BDS).

Energy Component	4c-AChE	7b-BChE	Donepezil-AChE	Tacrine-BChE
ΔG_{gas}	-22.75	-28.76	-26.85	-28.26
ΔG_{solv}	9.65	16.27	11.38	11.54
ΔG_{Total}	-13.11	-12.49	-15.47	-16.72

newly synthesized compounds to Lipinski's rule of five was evaluated [47]. Besides topological polar surface area (TPSA) and the number of rotatable bonds (# Rot. B) have been linked to drug bioavailability [48–52]. Consequently, computational values of the molecular properties of the studied compounds were calculated using the *Molsoft* and *Molinspiration* software and compared to the values of the reference drug, donepezil (SI: Table S5). The molecular characteristics that prove adequate inhibitory activity against AChE and BChE are summarized in

Table 5.

As clear from the results, the studied compounds possess TPSA values = 35.58–109.11 Å², which is less than the maximal limit ~ 140 Å², showing good intestinal absorption. Furthermore, all compounds under investigation have 5–9 rotatable bonds, which might show good oral bioavailability. It has been shown that for the compound to have a reasonable probability of being well absorbed, the Log P value must be in the range of -0.4 to 5 [52]. On this basis, the listed Log P values (Table 5) of the tested compounds (1.32, - 5.14) afford good evidence for acceptable levels of bioavailability.

The blood-brain barrier (BBB) protects the brain from the toxic side effects of drugs and exogenous molecules. However, it is crucial that medications developed for neurological disorders cross into the brain in therapeutic concentrations. In a trial for modeling BBB scores, an algorithm has been developed based on a list of physicochemical descriptors. This is based on five physicochemical descriptors involving the number of aromatic rings, heavy atoms: a descriptor consisting of molecular weight, hydrogen bond donor, and hydrogen bond acceptors

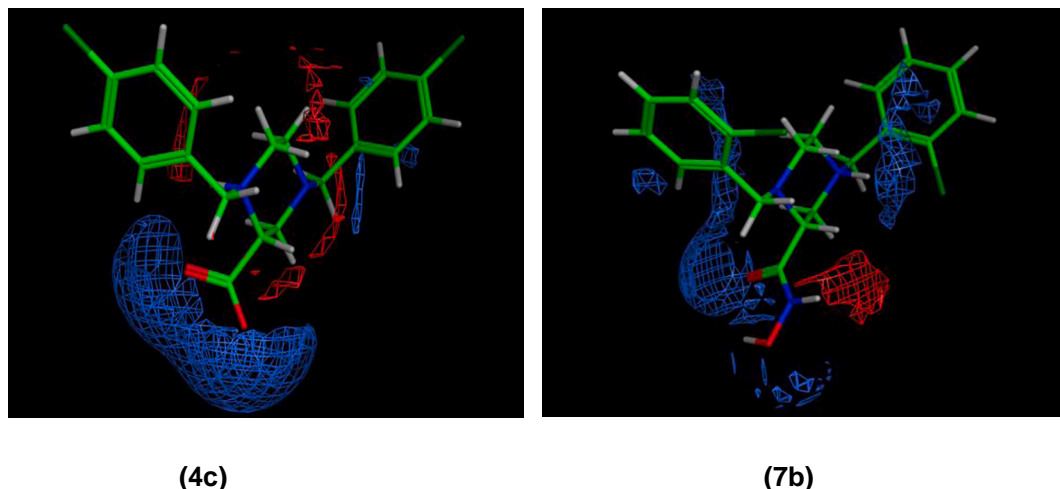


Fig. 8. The Molecular Electrostatic Potential Maps of compounds **4c** and **7b**.

Table 5

Computational molecular characteristics of the most active compounds comparison to Donepezil.

Code	MWt.	cLogP (o/w)	TPSA (Å ²)	# Rot. B	Lip. Viol.	BBB	Drug likeness score
Donpz.	379.5	4.46	32.39	6	0	5.29	1.56
4b	379.29	3.21	43.78	5	0	4.91	0.16
4c	379.29	3.46	43.78	5	0	4.91	0.30
4f	430.50	1.32	80.70	9	0	3.20	0.54
5b	393.32	2.33	61.60	6	0	4.21	0.69
5c	393.32	2.57	61.60	6	0	4.21	0.86
6a	366.49	3.63	72.19	5	0	4.61	0.04
6b	435.38	4.56	72.19	5	0	4.66	0.36
6c	435.38	4.81	72.19	5	0	4.66	0.42
6f	486.59	2.67	109.11	9	0	3.04	0.61
7b	394.30	2.54	55.81	6	0	4.48	0.64
7c	394.30	2.78	55.81	6	0	4.48	0.80
7d	361.39	1.72	55.81	6	0	4.41	0.57
7e	385.46	1.51	74.27	8	0	3.26	0.56
8a	337.47	2.83	35.58	7	0	5.20	0.64
8b	385.51	3.92	35.58	7	0	4.79	0.51
8f	391.56	4.21	35.58	7	0	5.14	0.55
8i	459.18	5.14	35.58	7	1	5.04	0.81

cLogP: lipophilicity parameter; **TPSA**: topological polar surface area (<140 Å²); # rot B: number of rotatable bonds (<10); # violation of Lipinski's rule of 5; **BBB**: The Blood-Brain Barrier (BBB) Score: 6-High, 0-Low [53]. **Drug likeness score**: -0.5 – 1.5.

(MWHBN), TPSA, and pKa. According to the study results, it has been said that compounds with BBB scores up to 6 are defined as high probability of penetration BBB, and those with a score of 0 or lower as low [53]. The results of the studied compounds, (Table 5), show BBB score values ranging from 3.04 to 5.20, which are closely related to that of the reference drug, Donepezil (5.29), illustrating enhanced potential for penetrating the BBB. Drug likeness is a qualitative concept used in drug design for how “druglike” a substance is; concerning factors like -bioavailability. A drug's likeness stands for a complex balance of various molecular properties and structural features. According to *Molinspiration* virtual screening engine, molecules having score values ranging from -0.5 to 1.5 are considered drug-like. The results of the studied compounds (Table 5), show drug likeness scores ranging from 0.04 to 0.86, implying acceptable bioavailability.

3. Conclusion

New series of 1,4-bisbenzylpiperazine-2-carboxylic acid derivatives **3-5(a-g)**, **7a-f**, **8a-s** and the corresponding -2-(1,3,4-oxadiazole-2-thiones) **6a-g** have been developed to target the multifaceted nature of AD. These compounds were evaluated *in vitro* and *in silico* against both AChE and BChE. Most of the synthesized compounds effectively inhibited the targeted enzymes in the μM to nM range *in vitro*. SAR analysis revealed clear selectivity for AChE inhibition by the carboxylic acid series **4a-g**. Furthermore, modification of the parent acids to the carbonylhydrazides, **5a-g** results in a slight decrease of the inhibitory effects. However, cyclization of the carbonylhydrazide to the respective 1,3,4-oxadiazole-2-thiones **6a-g** shows comparable inhibitory effects to the parent acids. Conversely, the hydroxamic acids **7a-f** and the carboxamides **8a-s** showed promising selectivity and enhanced inhibitory potency against BChE. Predominantly, compound **7b**, 1,4-bis(2-chlorobenzyl)-piperazine-2-hydroxamic acid, displayed nanomolar inhibitory activity against BChE ($K_i = 1.62 \pm 0.08 \text{ nM}$; $SI = 21862.5$). The results show that EWGs on the benzyl moiety enhanced inhibitory activity compared to the EDGs. Molecular dynamic simulations of the hit compounds **4c** and **7b** demonstrate good binding stability inside the active sites of both AChE and BChE along 50-ns. In summary, these findings are a good motivation for further optimization in the management of Alzheimer's disease.

3.1. STDF acknowledgment

This paper is based upon work supported by Science, Technology & Innovation Funding Authority (STDF) under Post-Graduate Support Grant (PGSG) (ID 44589, call 1).

4. Experimental

4.1. Chemistry

Solvents and reagents were bought from Sigma-Aldrich and Fisher Scientific companies. Solvents were dried according to standard methods. TLC checked the chemical reactions using commercially available alumina plates coated with silica gel 60 F254 (Merck). The structures of the synthesized compounds were confirmed by IR, ¹H NMR, ¹³C NMR, and Mass spectroscopy. ¹H NMR spectra were recorded on a 400 MHz AVANCE-III High-Performance FT-NMR spectrometer (Bruker Biospin International AG, Switzerland). ¹³C NMR spectra were achieved using AVANCE-III High-Performance FT-NMR spectrum (100 MHz) (Bruker Biospin International AG, Switzerland) at the Faculty of Science-Zagazig University, Zagazig/Egypt. The chemical shifts are reported in ppm downfield from TMS, and coupling constants are reported in hertz (Hz). Proton coupling patterns are abbreviated as singlet (s), doublet (d), triplet (t) and multiplet (m). Mass spectra were recorded on a JEOL® mass spectrometer at the faculty of Science-Assiut University, Assiut, Egypt. Elemental analyses were performed on Perkin Elmer 2400 CHN elemental analyzer, and the found were within $\pm 0.4 \%$ of the calculated values, at the regional center for mycology and biotechnology (Al Azhar University, Cairo/Egypt). The following intermediates were synthesized through applying the assigned reported methods and their characteristics match the cited values: **1 (a, c)** [25]; **1 (b, d, e, g)** [54]; **1 (b, f)** [55]; **2 (a, b, e, g)** [56]; **2 (c, d)** [57]; **2f** [58].

4.1.1. Ethyl 1,4-dibenzylpiperazine-2-carboxylate derivatives 3a-g

Ethyl 2,3-dibromopropionate (3.6 mL, 25 mmol) was added dropwise to a hot solution of the appropriate N^1, N^2 -dibenzylethane-1,2-diamine **2a-g** (20 mmol), and triethylamine (9 mL, 65 mmol), in dry toluene (200 mL). The mixture was refluxed overnight and tracked with TLC (CH₂Cl₂:CH₃OH; 98:2). The reaction mixture was cooled, washed with aqueous NaHCO₃ (3 \times 25 mL) and brine (2 \times 25 mL). The organic layer was dried over anhydrous MgSO₄, filtered, and evaporated under reduced pressure. The products were purified by column chromatography (CC), using gradient elution of CH₂Cl₂:CH₃OH, as assigned below.

4.1.1.1. Ethyl 1,4-dibenzylpiperazine-2-carboxylate 3a. Yield: 79 %, m.p: 56 – 58 °C (lit: yellow oil) [59]. IR (ν_{max} , cm⁻¹): 1731 (C=O), 1223 (C–N), 1193 (C–O–C). ¹H NMR (400 MHz, DMSO-*d*₆) δ : 1.12(t, $J = 7.2 \text{ Hz}$, 3H, CH₂CH₃), 2.25–2.55 (m, 4H, piperazine), 2.73(m, 1H, piperazine), 3.01(m, 1H, piperazine), 3.31(m, 1H, CH-piperazine), 3.36 (d, $J = 13.6 \text{ Hz}$, 1H, CH₂Ph), 3.52 (d, $J = 13.2 \text{ Hz}$, 1H, CH₂Ph), 3.61 (d, $J = 13.2 \text{ Hz}$, 1H, CH₂Ph), 3.84 (d, $J = 13.6 \text{ Hz}$, 1H, CH₂Ph), 4.07(q, $J = 7.2 \text{ Hz}$, 2H, CH₂CH₃), 7.18–7.34 (m, 10H, Ar). ¹³C NMR (100 MHz, DMSO-*d*₆) δ : 171.2, 138.6, 138.0, 128.6 (2C), 128.5 (2C), 128.2 (2C), 128.1 (2C), 126.9 (2C), 61.7, 59.8, 58.6, 54.9, 52.8 (2C), 47.4, 14.1. **Anal.** Calc. for C₂₁H₂₆N₂O₂ (338.44): C, 74.52; H, 7.74; N, 8.28. Found: C, 74.31; H, 7.85; N, 8.50.

4.1.1.2. Ethyl 1,4-bis-(2-chlorobenzyl) piperazine-2-carboxylate 3b. Yield: 78 %, yellow oil (CC; CH₂Cl₂:CH₃OH: 98.5: 1.5 %). ¹H NMR (400 MHz, DMSO-*d*₆) δ : 1.11 (t, $J = 7.2 \text{ Hz}$, 3H, CH₂CH₃), 2.31 (m, 1H, piperazine), 2.43 (m, 2H, piperazine), 2.62 (d, $J = 11.2 \text{ Hz}$, 1H, piperazine), 2.94 (d, $J = 12 \text{ Hz}$, 1H, piperazine), 3.10 (t, $J = 11.2 \text{ Hz}$, 1H, piperazine), 3.45–3.59 (m, 3H, CH₂Ph, CH-piperazine), 3.80 (d, $J = 15.2 \text{ Hz}$, 1H, CH₂Ph), 3.96 (d, $J = 14.8 \text{ Hz}$, 1H, CH₂Ph), 4.07 (q, $J = 7.2 \text{ Hz}$, 2H, CH₂CH₃), 7.23–7.34 (m, 4H, Ar), 7.37–7.43 (m, 3H, Ar-H), 7.49

(dd, $J = 1.6$ Hz, $J = 7.2$ Hz, 1H, Ar). ^{13}C NMR (100 MHz, DMSO- d_6) δ : 171.2, 136.3, 135.4, 133.3, 133.0, 130.6, 130.2, 129.2, 128.6, 128.4, 127.0, 126.8, 61.3, 59.7, 58.3, 55.6, 55.1, 52.9, 46.9, 14.0. **Anal.** Calc. for $\text{C}_{21}\text{H}_{24}\text{Cl}_2\text{N}_2\text{O}_2$ (407.33): C, 61.92; H, 5.94; N, 6.88. Found: C, 61.78; H, 6.07; N, 7.12. **MS:** $[\text{M}]^+$: 407.69(28.59 %); M^{+2} : 409.31 (23.01 %); base peak: 335.19 (100 %).

4.1.1.3. Ethyl 1,4-bis-(4-chlorobenzyl) piperazine-2-carboxylate 3c. Yield: 77 % (CC: CH_2Cl_2 : CH_3OH 98.5:1.5 %), m.p.:70–73 °C (lit.m. p:76–78 °C) [59]. IR ν cm^{-1} : 1732 (C=O), 1195 (C–O–C), 1156 (C–N). ^1H NMR (400 MHz, DMSO- d_6) δ : 1.13 (t, $J = 7.2$ Hz, 3H, CH_2CH_3), 2.31 (m, 2H, piperazine), 2.41 (m, 1H, piperazine), 2.70 (m, 1H, piperazine), 2.97 (m, 1H, piperazine), 3.32 (m, 1H, piperazine), 3.36 (m, 1H, CH -piperazine), 3.52 (d, $J = 13.6$, 2H, CH_2Ph), 3.61 (d, $J = 13.6$ Hz, 1H, CH_2Ph), 3.82 (d, $J = 14$ Hz, 1H, CH_2Ph), 4.07 (q, $J = 7.2$ Hz, 2H, CH_2CH_3), 7.23–7.38 (m, 8H, Ar). ^{13}C NMR (100 MHz, DMSO- d_6) δ : 171.7, 138.3, 137.6, 131.9, 131.9, 130.8 (2C), 130.7 (2C), 128.6 (2C), 128.5 (2C), 61.1, 60.3, 58.2, 55.3, 53.2, 49.1, 47.7, 14.5. **Anal.** Calc. for $\text{C}_{21}\text{H}_{24}\text{Cl}_2\text{N}_2\text{O}_2$ (407.33): C, 61.92; H, 5.94; N, 6.88. Found: C, 61.98; H, 6.13; N, 7.05.

4.1.1.4. Ethyl 1,4-bis-(4-fluorobenzyl) piperazine-2-carboxylate 3d. Yield: 68 %, (CC: CH_2Cl_2 : CH_3OH 97:3%), m.p.:49–50 °C (lit.m. p:46–48 °C) [59]. IR ν cm^{-1} (KBr): 1732 (C=O), 1255 (C–N), 1222 (C–O–C ester). ^1H NMR (400 MHz, DMSO- d_6) δ : 1.14 (t, $J = 7.2$ Hz, 3H, CH_2CH_3), 2.40 (m, 4H, piperazine), 2.72 (m, 1H, piperazine), 2.98 (m, 1H, piperazine), 3.33 (m, 1H, CH -piperazine), 3.34 (m, 1H, CH_2Ph), 3.53 (d, $J = 13.6$ Hz, 1H, CH_2Ph), 3.62 (d, $J = 13.2$ Hz, 1H, CH_2Ph), 3.84 (d, $J = 13.6$ Hz, 1H, CH_2Ph), 4.08 (q, $J = 7.2$ Hz, 2H, CH_2CH_3), 7.17–7.07 (t, $J_{\text{H-F}} = 8.8$ Hz, 4H, Ar), 7.23–7.36 (m, 4H, Ar). ^{13}C NMR (100 MHz, DMSO- d_6) δ : 171.2, 162.5, 160.1, 134.7, 134.1, 130.4 (2C), 130.3 (2C), 114.9 (2C), 114.7 (2C), 61.6, 60.7, 59.7, 57.7, 54.8, 52.7, 47.3, 14.0. **Anal.** Calc. for $\text{C}_{21}\text{H}_{24}\text{F}_2\text{N}_2\text{O}_2$ (374.42): C, 67.36; H, 6.46; N, 7.48. Found: C, 67.20; H, 6.72; N, 7.69.

4.1.1.5. Ethyl 1,4-bis-(4-methoxybenzyl) piperazine-2-carboxylate 3e. Yield:71 %, orange oil [59], (CC: CH_2Cl_2 : CH_3OH 98:2%). ^1H NMR (400 MHz, DMSO- d_6) δ : 1.13 (t, $J = 7.2$ Hz, 3H, CH_2CH_3), 2.38 (m, 4H, piperazine), 2.65 (m, 1H, piperazine), 2.95 (m, 1H, piperazine), 3.25 (m, 1H, CH -piperazine), 3.28 (d, $J = 13.2$ Hz, 1H, CH_2Ph), 3.43 (d, $J = 13.2$ Hz, 1H, CH_2Ph), 3.53 (d, $J = 13.2$ Hz, 1H, CH_2Ph), 3.71 (s, 6H, 2 \times OCH_3), 3.75(d, $J = 12.8$ Hz, 1H, CH_2Ph), 4.07(q, $J = 7.2$ Hz, 2H, CH_2CH_3), 6.86 (m, 4H, Ar), 7.14 (d, $J = 8.8$ Hz, 2H, Ar), 7.18 (d, $J = 8.8$ Hz, 2H, Ar). ^{13}C NMR (100 MHz, DMSO- d_6) δ : 171.3, 158.3 (2C), 130.2, 129.9 (2C), 129.8 (2C), 129.7, 113.6 (2C), 113.5 (2C), 61.6, 61.0, 59.8, 57.9, 55.0 (2C), 54.8, 52.6, 47.4, 14.1. **Anal.** Calc. for $\text{C}_{23}\text{H}_{30}\text{N}_2\text{O}_4$ (398.50): C, 69.32; H, 7.59; N, 7.03. Found: C, 69.16; H, 7.75; N, 7.20.

4.1.1.6. Ethyl 1,4-bis-(3,4-dimethoxybenzyl) piperazine-2-carboxylate 3f. Yield: 78 %, (CC: CH_2Cl_2 : CH_3OH 99:1%), m.p.:87–90°C. ^1H NMR (400 MHz, DMSO- d_6) δ : 1.14 (t, $J = 7.2$ Hz, 3H, CH_2CH_3), 2.36 (m, 3H, piperazine), 2.67 (m, 1H, piperazine), 2.98 (m, 1H, piperazine), 3.25 (m, 1H, piperazine), 3.26 (m, 1H, CH -piperazine), 3.28 (m, 1H, CH_2Ph), 3.46 (d, $J = 13.2$ Hz, 1H, CH_2Ph), 3.55 (m, 1H, CH_2Ph), 3.72 (s, 12H, 4 \times OCH_3), 3.76 (d, $J = 13.2$ Hz, 1H, CH_2Ph), 4.08 (q, $J = 7.2$ Hz, 2H, CH_2CH_3), 6.71–6.90 (m, 6H, Ar). ^{13}C NMR (100 MHz, DMSO- d_6) δ : 171.4, 148.6, 148.6 (2C), 147.8, 130.7, 130.3, 120.7, 120.6, 112.3, 112.2, 61.4, 59.7, 58.2, 55.5 (2C), 55.4 (3C), 54.8, 52.7, 52.2, 14.1. **Anal.** Calc. for $\text{C}_{25}\text{H}_{34}\text{N}_2\text{O}_6$ (458.55): C, 65.48; H, 7.47; N, 6.11. Found: 65.70; H, 7.65; N, 6.39.

4.1.1.7. Ethyl 1,4-bis(4-dimethylaminobenzyl) piperazine-2-carboxylate 3g. Yield:57 %; orange oil (CC, CH_2Cl_2 : CH_3OH , 95:5%). ^1H NMR (400 MHz, DMSO- d_6) δ : 1.14 (t, $J = 7.2$ Hz, 3H, CH_2CH_3), 2.29 (m, 2H, piperazine), 2.38 (m, 2H, piperazine), 2.81 (m, 1H, piperazine), 2.84 (s,

12H, 4 \times CH_3), 2.92 (m, 1H, piperazine), 3.17 (m, 1H, CH -piperazine), 3.23 (d, $J = 12.8$ Hz, 1H, CH_2Ph), 3.37 (d, $J = 12.8$ Hz, 2H, CH_2Ph), 3.68 (d, $J = 13.2$ Hz, 1H, CH_2Ph), 4.07 (q, $J = 7.2$ Hz, 2H, CH_2CH_3), 6.63 (dd, $J = 8.8$ Hz, $J = 2$ Hz, 4H, Ar), 7.00–7.07 (t, $J = 8.8$ Hz, 4H, Ar). ^{13}C NMR (100 MHz, DMSO- d_6) δ : 171.4, 149.6 (2C), 129.6 (2C), 129.5 (2C), 125.4, 125.1, 112.2 (2C), 112.1 (2C), 61.4, 59.8, 58.1, 54.9, 54.8, 52.6, 47.7, 40.2 (4C), 14.0. **Anal.** Calc for $\text{C}_{25}\text{H}_{36}\text{N}_4\text{O}_2$ (424.58): C, 70.72; H, 8.55; N, 13.20. Found: C, 70.51; H, 8.72; N, 13.43. **MS:** $[\text{M}]^+$:424.47 (32 %); base peak: 134.2 (100 %).

4.1.2. 1,4-Dibenzylpiperazine-2-carboxylic acid derivatives 4a–g

Method (A): To a solution of ethyl 1,4-bis-(un/substituted benzyl) piperazine-2-carboxylate **3(a–g)** (8 mmol) in dioxane (10 mL) was added 2 ml aqueous NaOH (1 M) and the mixture refluxed for 2 h. The solvent was evaporated under reduced pressure and the residue was dissolved in water and acidified with 1 N HCl dropwise until a precipitate formed. This was then filtered, washed with water, dried, and recrystallized from ether.

Method (B): 2,3-dibromopropionic acid (1.5 g, 6.5 mmol) was added to a hot solution of N^1, N^2 -dibenzylethan-1,2-diamines **2a–g** (6.5 mmol) in toluene (60 ml) and triethylamine (3.1 mL, 22.7 mmol), and the mixture was refluxed overnight. After cooling to 0 °C, the precipitate formed was filtered, washed with ether, then water, dried, and recrystallized from ether.

4.1.2.1. 1,4-Dibenzylpiperazine-2-carboxylic acid 4a. Yield: 61 % (A), 76 % (B), m.p: 125–128 °C. IR (KBr) ν_{max} cm^{-1} : 3416 (OH), 1627 (C=O), 1224 (C–N). ^1H NMR (400 MHz, DMSO- d_6) δ : 2.34 (m, 1H, piperazine), 2.38 (m, 1H, piperazine), 2.57 (m, 1H, piperazine), 2.63 (m, 1H, piperazine), 2.90 (m, 1H, piperazine), 3.16 (m, 1H, piperazine), 3.19 (m, 1H, CH -piperazine), 3.47 (d, $J = 12.8$ Hz, 1H, CH_2Ph), 3.58 (d, $J = 12.8$ Hz, 2H, CH_2Ph), 3.87 (d, $J = 14$ Hz, 1H, CH_2Ph), 7.21–7.36 (m, 10H, Ar). ^{13}C NMR (100 MHz, DMSO- d_6) δ : 172.7, 138.0 (2C), 129.4 (2C), 129.3 (2C), 128.7 (2C), 127.7 (2C), 127.5 (2C), 61.9 (2C), 58.9, 55.3, 52.5, 48.3. **Anal.** Calc. for $\text{C}_{19}\text{H}_{22}\text{N}_2\text{O}_2$ (310.39): C, 73.52; H, 7.14; N, 9.03. Found: C, 73.29; H, 7.26; N, 9.21.

4.1.2.2. 1,4-Bis(2-chlorobenzyl) piperazine-2-carboxylic acid 4b. Yield: 68 % (A), 79 % (B), m.p: 185–187 °C. ^1H NMR (400 MHz, DMSO- d_6) δ : 2.31–2.51 (m, 4H, piperazine), 2.60 (m, 1H, piperazine), 2.79 (m, 1H, piperazine), 2.98 (m, 1H, CH -piperazine), 3.56 (s, 2H, CH_2Ph), 3.68 (m, 1H, CH_2Ph), 3.97 (d, $J = 14.4$ Hz, 1H, CH_2Ph), 7.31 (m, 4H, Ar), 7.40 (t, $J = 8.8$ Hz, 2H, Ar), 7.47 (d, $J = 7.2$ Hz, 1H, Ar), 7.57 (d, $J = 8$ Hz, 1H, Ar). ^{13}C NMR (100 MHz, DMSO- d_6) δ : 173.2, 136.5, 135.3, 133.2, 133.0, 130.7, 130.3, 129.2, 129.1, 128.6, 128.3, 127.0, 126.9, 62.4, 58.3, 55.6, 55.5, 52.7, 47.6. **Anal.** Calc. for $\text{C}_{19}\text{H}_{20}\text{Cl}_2\text{N}_2\text{O}_2$ (379.28): C, 60.17; H, 5.32; N, 7.39. Found: C, 60.40; H, 5.51; N, 7.58.

4.1.2.3. 1,4-Bis(4-chlorobenzyl) piperazine-2-carboxylic acid 4c. Yield:76 % (A), 87 % (B), m.p: 193–194 °C. ^1H NMR (400 MHz DMSO- d_6 , TFA- d_1) δ : 2.80 (m, 1H, piperazine), 3.21 (m, 4H, piperazine), 3.47 (m, 1H, piperazine), 3.82 (m, 2H, CH_2Ph , CH -piperazine), 4.09 (d, $J = 12$ Hz, 1H, CH_2Ph), 4.31 (d, $J = 12$ Hz, 2H, CH_2Ph), 7.43 (m, 4H, Ar), 7.53 (m, 4H, Ar), 10.17 (br. s, 1H, COOH, exchangeable). ^{13}C NMR (100 MHz, DMSO- d_6) δ : 173.1, 137.9, 137.2, 132.1, 132.0, 131.0 (2C), 130.9 (2C), 128.6 (4C), 62.5, 61.0, 58.2, 55.4, 52.7, 48.1. **Anal.** Calc. for $\text{C}_{19}\text{H}_{20}\text{Cl}_2\text{N}_2\text{O}_2$ (379.28): C, 60.17; H, 5.32; N, 7.39. Found: C, 60.43; H, 5.54; N, 7.61. **MS:** $[\text{M}]^+$: 379.77(70.15 %); M^{+2} : 380.66(42.57 %); base peak: 297.02:(100 %).

4.1.2.4. 1,4-Bis(4-fluorobenzyl) piperazine-2-carboxylic acid 4d. Yield: 75 % (A), 89 % (B), m.p:186–188 °C. IR ν_{max} cm^{-1} : 3424 (OH), 1620 (C=O), 1298 (C–N). ^1H NMR (400 MHz, DMSO- d_6) δ : 2.36 (m, 3H, piperazine), 2.59 (m, 2H, piperazine), 2.88 (m, 1H, piperazine), 3.20 (t, $J = 4.8$ Hz, 1H, CH -piperazine), 3.44 (m, 2H, CH_2Ph), 3.56 (d, $J = 13.2$

H_z, 1H, CH₂Ph), 3.84 (d, *J* = 13.2 Hz, 1H, CH₂Ph), 7.08–7.19 (td, *J*_{H-F} = 9.2 Hz, *J* = 2.6 Hz, 4H, Ar), 7.26–7.38 (m, 4H, Ar). ¹³C NMR (100 MHz, DMSO-*d*₆) δ: 172.6, 162.3, 160.1, 134.4, 133.9, 130.6 (2C), 130.5 (2C), 115.0 (2C), 114.8 (2C), 62.1, 60.6, 57.7, 54.9, 52.2, 47.6. **Anal.** Calc. for C₁₉H₂₀F₂N₂O₂ (346.37): C, 65.88; H, 5.82; N, 8.09. Found: C, 65.62; H, 6.01; N, 8.36. **MS:** [M]⁺ 346.60 (30.48 %); base peak: 296.37(100 %).

4.1.2.5. 1,4-Bis(4-methoxybenzyl) piperazine-2-carboxylic acid 4e. Yield: 73 % (A), 81 % (B), white powder, m.p: 228–230 °C. IR ν_{max} (KBr) cm⁻¹: 3425 (COOH), 1613 (C=O), 1305 (C–N), 1183 (C–O–C). ¹H NMR (400 MHz, DMSO-*d*₆, TFA-*d*₁) δ: 3.29–3.49 (m, 5H, piperazine), 3.75 (s, 3H, OCH₃), 3.76 (s, 3H, OCH₃), 3.80 (m, 1H, piperazine), 4.17 (d, *J* = 13.8 Hz, 1H, CH-piperazine), 4.40 (m, 3H, CH₂Ph, CH₂Ph), 4.50 (d, *J* = 13.2 Hz, 1H, CH₂Ph), 6.98 (dd, *J* = 8.8 Hz, *J* = 2 Hz, 4H, Ar), 7.40 (d, *J* = 8.4 Hz, 2H, Ar), 7.50 (d, *J* = 8.4 Hz, 2H, Ar), 9.52 (br. s, 1H, COOH, exchangeable). ¹³C NMR (100 MHz, DMSO-*d*₆) δ: 167.1, 160.7, 160.6, 133.5, 133.0, 132.0, 120.9, 119.8, 117.0, 114.6, 114.4, 114.0, 111.2, 58.3, 55.4 (2C), 50.2, 48.9, 46.9, 42.3, 42.9. **Anal.** Calc. for C₂₁H₂₆N₂O₄ (370.44): C, 68.09; H, 7.07; N, 7.56. Found: C, 67.87; H, 7.24; N, 7.80.

4.1.2.6. 1,4-Bis(3,4-dimethoxybenzyl) piperazine-2-carboxylic acid 4f. Yield: 67 % (A), 74 % (B), white powder, m.p: 202–204 °C. ¹H NMR (400 MHz, DMSO-*d*₆) δ: 3.05–2.38 (m, 5H, piperazine), 3.37 (d, *J* = 12.8 Hz, 1H, piperazine), 3.46 (d, *J* = 13.6 Hz, 1H, CH-piperazine), 3.60 (d, *J* = 12.8 Hz, 2H, CH₂Ph), 3.73 (s, 12H, 4 × OCH₃), 3.88 (d, *J* = 13.8 Hz, 2H, CH₂Ph), 7.10–6.74 (m, 6H, Ar). ¹³C NMR (100 MHz, DMSO-*d*₆) δ: 172.7, 149.1 (2C), 148.5, 148.3, 130.5, 130.2, 121.6, 121.3, 113.1, 112.8, 112.0, 111.9, 61.7, 60.2, 58.6, 56.0 (2C), 55.9 (2C), 55.1, 52.6, 49.1. **Anal.** Calc. for C₂₃H₃₀N₂O₆ (430.49): C, 64.17; H, 7.02; N, 6.51. Found: C, 63.98; H, 7.21; N, 6.68.

4.1.2.7. 1,4-Bis(4-dimethylaminobenzyl) piperazine-2-carboxylic acid 4g. Yield: 65 % (A), 76 % (B), m.p: 207–208 °C. ¹H NMR (400 MHz, DMSO-*d*₆, TFA-*d*₁) δ: 2.70 (m, 1H, piperazine), 2.92 (m, 1H, piperazine), 3.15 (s, 12H, 4 × CH₃), 3.52 (m, 3H, piperazine), 3.77 (m, 1H, piperazine), 4.02 (m, 1H, CH-piperazine), 4.26 (m, 1H, CH₂Ph), 4.38 (m, 2H, CH₂Ph), 4.60 (m, 1H, CH₂Ph), 7.85–7.10 (m, 8H, Ar). ¹³C NMR (100 MHz, DMSO-*d*₆) δ: 167.2, 142.8, 142.0, 130.8, 121.4, 119.8 (2C), 117.0 (2C), 114.1 (2C), 111.3 (2C), 53.4, 52.9, 47.3, 46.3 (4C), 46.0, 42.5, 41.9. **Anal.** Calc. for C₂₃H₃₂N₄O₂ (396.53): C, 69.67; H, 8.13; N, 14.13. Found: C, 69.85; H, 8.30; N, 14.39.

4.1.3. 1,4-Dibenzylpiperazine-2-carbohydrazides 5a-g

Hydrazine hydrate (99 %) (0.4 mL/12.5 mmol) was added dropwise to a hot solution of the respective ethyl 1,4-dibenzylpiperazine-2-carboxylate derivative, **3a-g**, (2.5 mmol) in ethanol (5 mL). The reaction was refluxed overnight, allowed to cool to room temperature, and then poured into crushed ice. The precipitate formed was filtered, washed with water, dried, and then washed with diethyl ether.

4.1.3.1. 1,4-Dibenzylpiperazine-2-carbohydrazide 5a. Yield: 74 %, m. p: 93–95 °C. IR max, cm⁻¹: 3311 (NH & NH₂), 1626(C=O), 1148 (CN of Carbohydrazide), 1120 (C–N of piperazine ring). ¹H NMR (400 MHz, DMSO-*d*₆) δ: 1.97 (m, 2H, piperazine), 2.10 (m, 1H, piperazine), 2.50 (m, 3H, piperazine), 2.78 (d, *J* = 11.2 Hz, CH-piperazine), 2.98 (d, *J* = 12.8 Hz, 1H, CH₂Ph), 3.29 (d, *J* = 12 Hz, 1H, CH₂Ph), 3.39 (d, *J* = 13.2 Hz, 1H, CH₂Ph), 3.60 (d, *J* = 13.6 Hz, 1H, CH₂Ph), 4.14 (br. s, 2H, NHNH₂, exchangeable), 7.08–7.26 (m, 10H, Ar), 9.01 (br. s, 1H, NHNH₂, exchangeable). ¹³C NMR (100 MHz, DMSO-*d*₆) δ: 170.1, 138.0, 137.8, 128.9 (2C), 128.2 (2C), 128.1 (2C), 127.0 (2C), 126.9 (2C), 64.8, 61.8, 58.8, 55.5, 52.2, 50.0. **Anal.** Calc. for C₁₉H₂₄N₄O (324.42): C, 70.34; H, 7.46; N, 17.27. Found: C, 70.51; H, 7.63; N, 17.41.

4.1.3.2. 1,4-Bis(2-chlorobenzyl) piperazine-2-carbohydrazide 5b. Yield:

72 %, m. p: 104–106 °C. ¹H NMR (400 MHz, DMSO-*d*₆) δ: 2.19 (m, 1H, piperazine), 2.30 (m, 1H, piperazine), 2.44 (m, 1H, piperazine), 2.55–2.75 (m, 3H, piperazine), 3.05 (m, 1H, CH-piperazine), 3.39–3.68 (m, 4H, 2 × CH₂Ph), 4.25 (br. s, 2H, NHNH₂, exchangeable), 7.24–7.47 (m, 7H, Ar), 7.62 (dd, *J* = 7.6 Hz, *J* = 1.6 Hz, 1H, Ar), 9.12 (br. s, 1H, NHNH₂, exchangeable). ¹³C NMR (100 MHz, DMSO-*d*₆) δ: 170.4, 136.1, 136.6, 133.9, 133.4, 131.6, 131.2, 129.8, 129.5, 129.3, 129.0, 127.6, 127.5, 64.8, 58.9, 55.8, 55.8, 52.6, 50.4. **Anal.** Calc. for C₁₉H₂₂Cl₂N₄O (393.31): C, 58.02; H, 5.64; N, 14.24. Found: C, 58.29; H, 5.88; N, 14.51. **MS:** [M]⁺: 393.62(100 %); M⁺²: 395.48(50.94 %).

4.1.3.3. 1,4-Bis(4-chlorobenzyl) piperazine-2-carbohydrazide 5c. Yield: 78 %, m.p: 84–86 °C. IR ν_{max}, cm⁻¹: 3302 (NH, NH₂), 1678 (C=O), 1489 (C–N of carbo-hydrazide), 1090 (C–N of piperazine). ¹H NMR (400 MHz, DMSO-*d*₆) δ: 2.09 (m, 2H, piperazine), 2.22 (m, 1H, piperazine), 2.54–2.65 (m, 3H, piperazine), 2.92 (m, 1H, CH-piperazine), 3.10 (d, *J* = 14 Hz, 1H, CH₂Ph), 3.48 (d, *J* = 13.2 Hz, 2H, CH₂Ph), 3.67 (d, *J* = 14 Hz, 1H, CH₂Ph), 4.24 (br. s, 2H, NHNH₂, exchangeable), 7.25–7.40 (m, 8H, Ar), 9.15 (br. s, 1H, NHNH₂, exchangeable). ¹³C NMR (100 MHz, DMSO-*d*₆) δ: 170.6, 137.7, 137.3, 132.0 (2C), 131.9 (2C), 131.2 (2C), 128.6 (2C), 128.5 (2C), 65.1, 61.2, 58.3, 55.8, 52.5, 50.4. **Anal.** Calc. for C₁₉H₂₂Cl₂N₄O (393.31): C, 58.02; H, 5.64; N, 14.24. Found: C, 58.27; H, 5.83; N, 14.57.

4.1.3.4. 1,4-Bis(4-fluorobenzyl) piperazine-2-carbohydrazide 5d. Yield: 75 %, m.p: 74–75 °C. ¹H NMR (400 MHz, DMSO-*d*₆) δ: 2.04–2.30 (m, 3H, piperazine), 2.55–2.76 (m, 3H, piperazine), 2.95 (m, 1H, CH-piperazine), 3.15 (d, *J* = 13.6 Hz, 1H, CH₂Ph), 3.44 (d, *J* = 12.8 Hz, 1H, CH₂Ph), 3.53 (d, *J* = 12.8 Hz, 1H, CH₂Ph), 3.73 (d, *J* = 13.2 Hz, 1H, CH₂Ph), 4.29 (br. s, 2H, NHNH₂, exchangeable), 7.07–7.19 (t, *J*_{H-F} = 8.8 Hz, 4H, Ar), 7.28–7.39 (m, 4H, Ar), 9.17 (br. s, 1H, NHNH₂, exchangeable). ¹³C NMR (100 MHz, DMSO-*d*₆) δ: 170.5, 163.0, 160.6, 134.7, 134.4, 131.2 (2C), 131.2 (2C), 115.5, 115.3, 115.2, 115.1, 65.1, 61.3, 58.3, 55.8, 52.5, 50.3. **Anal.** Calc. for C₁₉H₂₂F₂N₄O (360.4): C, 63.32; H, 6.15; N, 15.55. Found: C, 63.04; H, 6.24; N, 15.73. **MS:** [M]⁺: 360.4 (5 %), base peak: 109.1 (100 %).

4.1.3.5. 1,4-Bis(4-methoxybenzyl) piperazine-2-carbohydrazide 5e. Yield: 76 %, m. p: 89–90 °C. IR ν_{max}, cm⁻¹: 3432 (NH₂), 3327 (NH), 1673 (C=O), 1250 (C–O–C), 1180 (C–N). ¹H NMR (400 MHz, DMSO-*d*₆) δ: 2.03 (m, 2H, piperazine), 2.14 (m, 1H, piperazine), 2.54–2.62 (m, 3H, piperazine), 2.84 (m, 1H, CH-piperazine), 3.00 (d, *J* = 12.8 Hz, 1H, CH₂Ph), 3.43 (d, *J* = 12.8 Hz, 2H, CH₂Ph), 3.63 (d, *J* = 12.8 Hz, 1H, CH₂Ph), 3.72 (s, 6H, 2 × OCH₃), 4.25 (br. s, 2H, NHNH₂, exchangeable), 6.82–6.88 (dd, *J* = 8.4 Hz, *J* = 3.2 Hz, 4H, Ar), 7.15 (d, *J* = 8 Hz, 2H, Ar), 7.20 (d, *J* = 8.4 Hz, 2H, Ar), 9.08 (br. s, 1H, NHNH₂, exchangeable). ¹³C NMR (100 MHz, DMSO-*d*₆) δ: 170.6, 158.5 (2C), 130.6 (2C), 130.5 (2C), 129.8, 129.7, 113.8 (2C), 113.7 (2C), 65.0, 61.4, 58.4, 55.4, 55.3, 52.3, 49.9. **Anal.** Calc. for C₂₁H₂₈N₄O₃ (384.47): C, 65.60; H, 7.34; N, 14.57. Found: C, 65.43; H, 7.51; N, 14.79.

4.1.3.6. 1,4-Bis(3,4-dimethoxybenzyl) piperazine-2-carbohydrazide 5f. Yield: 87 %, m.p: 102–105 °C. ¹H NMR (400 MHz, DMSO-*d*₆) δ: 2.10 (m, 2H, piperazine), 2.20 (m, 1H, piperazine), 2.53–2.71 (m, 3H, piperazine), 2.87 (m, 1H, CH-piperazine), 3.08 (d, *J* = 12.8 Hz, 1H, CH₂Ph), 3.35 (m, 1H, CH₂Ph), 3.41 (d, *J* = 12.8 Hz, 1H, CH₂Ph), 3.64 (d, *J* = 12 Hz, 1H, CH₂Ph), 3.74 (s, 12H, 4 × OCH₃), 4.26 (br. s, 2H, NHNH₂), 6.73–6.95 (m, 6H, Ar), 9.13 (br. s, 1H, NHNH₂, exchangeable). ¹³C NMR (100 MHz, DMSO-*d*₆) δ: 170.8, 148.9, 148.8, 148.3, 148.2, 130.4, 130.4, 121.7 (2C), 113.1, 113.0, 111.8, 111.7, 64.9, 61.9, 59.0, 55.9 (2C), 55.8 (2C), 55.5, 52.5, 50.1. **Anal.** Calc. for C₂₃H₃₂N₄O₅ (444.52): C, 62.14; H, 7.26; N, 12.60. Found: C, 61.98; H, 7.44; N, 12.87.

4.1.3.7. 1,4-Bis(4-(dimethylaminobenzyl) piperazine-2-carbohydrazide 5g. Yield: 71 %, m. p: 142–144 °C. ¹H NMR (400 MHz, DMSO-*d*₆) δ:

2.12–1.90(m, 3H, piperazine), 2.46 (m, 1H, piperazine), 2.57 (m, 2H, piperazine), 2.76 (m, 1H, CH-piperazine), 2.81(s, 12H, 4 × CH₃), 2.91(d, $J = 13.2$ Hz, 1H, CH₂Ph), 3.18 (d, $J = 12.8$ Hz, 1H, CH₂Ph), 3.34 (d, $J = 12.8$ Hz, 1H, CH₂Ph), 3.55 (d, $J = 12.8$ Hz, 1H, CH₂Ph), 4.21 (br. s, 2H, NHNH₂, exchangeable), 6.61(d, $J = 8$ Hz, 4H, Ar), 7.00 (d, $J = 8$ Hz, 2H, Ar), 7.04 (d, $J = 8$ Hz, 2H, Ar), 9.00 (br. s, 1H, NHNH₂, exchangeable). ¹³C NMR (100 MHz, DMSO-*d*₆) δ: 170.8, 150.1, 150.0, 130.3 (2C), 130.2 (2C), 125.5, 125.4, 112.6 (2C), 112.5 (2C), 66.3, 62.0, 58.9, 55.8, 52.6, 50.2, 40.7, 40.6. **Anal.** Calc. for C₂₃H₃₄N₆O (410.56): C, 67.29; H, 8.35; N, 20.47. Found: C, 67.05; H, 8.52; N, 20.63.

4.1.4. 5-(1,4-Disubstitutedbenzylpiperazin-2-yl)-1,3,4-oxadiazole-2(3H)-thione 6a-g

Carbon disulfide (0.3 mL, 5.3 mmol) was added to a hot solution of the respective 1,4-dibenzylpiperazine-2-carbohydrazide **5a-g**, (1.5 mmol) and KOH (0.08 g, 1.5 mmol) in methanol (10 mL). The reaction mixture was refluxed for 12 h until the evolution of H₂S ceased. The solvent was distilled off under reduced pressure and the residue dissolved in water and acidified with HCl. The precipitate was filtered, washed with water, dried, and recrystallized from methanol.

4.1.4.1. 5-(1,4-Dibenzylpiperazin-2-yl)-1,3,4-oxadiazole-2(3H)-thione 6a. Yield: 84 %, m.p: 109–111 °C. IR ν_{\max} , cm⁻¹: 3396 (NH), 1494 (C=N), 1454 (C=S), 1411 (C=N), 1377 (C=O), 1211 (C=N), 1144 (N=N). ¹H NMR (400 MHz, DMSO-*d*₆) δ: 2.32–2.50 (m, 3H, piperazine), 2.67 (m, 2H, piperazine), 2.86 (m, 1H, piperazine), 3.52 (m, 1H, CH-piperazine), 3.56 (m, 2H, CH₂Ph), 3.73 (d, $J = 13.6$ Hz, 1H, CH₂Ph), 3.88 (m, 1H, CH₂Ph), 7.21–7.39 (m, 10H, Ar). ¹³C-NMR (100 MHz, DMSO-*d*₆) δ: 177.8, 162.2, 137.8, 137.2, 128.7 (2C), 128.6 (2C), 128.2 (2C), 128.1 (2C), 127.1, 127.0, 61.2, 58.3, 56.1, 54.8, 52.1, 48.4. **Anal.** Calc. for C₂₀H₂₂N₄OS (366.48): C, 65.55; H, 6.05; N, 15.29; S, 8.75. Found: C, 65.38; H, 6.21; N, 15.43; S, 8.89. **MS:** [M]⁺: 366.51 (11.95 %); base peak: 313.29 (100 %).

4.1.4.2. 5-(1,4-Bis(2-chlorobenzyl) piperazin-2-yl)-1,3,4-oxadiazole-2(3H)-thione 6b. Yield: 77 %, m.p: 87 – 88 °C. ¹H NMR (400 MHz, DMSO-*d*₆) δ: 2.47 (m, 2H, piperazine), 2.56 (m, 1H, piperazine), 2.72 (m, 1H, piperazine), 2.84 (m, 1H, piperazine), 2.95 (m, 1H, piperazine), 3.59 (d, $J = 13.8$ Hz, 1H, CH₂Ph), 3.65 (d, $J = 13.2$ Hz, 1H, CH₂Ph), 3.76 (d, $J = 13.6$ Hz, 1H, CH₂Ph), 3.88 (d, $J = 14$ Hz, 1H, CH₂Ph), 4.04 (m, 1H, CH-piperazine), 7.25–7.36 (m, 4H, Ar), 7.37–7.45 (m, 3H, Ar), 7.50 (d, $J = 7.2$ Hz, 1H, Ar), 14.46 (br. s, 1H, NH, exchangeable). ¹³C NMR (100 MHz, DMSO-*d*₆) δ: 178.1, 162.7, 136.0, 135.6, 133.8, 133.6, 131.1, 130.9, 129.8, 129.7, 129.2 (2C), 127.5, 127.4, 58.6, 56.7, 55.9 55.5, 52.6, 48.4. **Anal.** Calc. for C₂₀H₂₀Cl₂N₄OS (435.37): C, 55.17; H, 4.63; N, 12.87; S, 7.36. Found: C, 55.43; H, 4.89; N, 13.08; S, 7.45.

4.1.4.3. 5-(1,4-Bis(4-chlorobenzyl) piperazin-2-yl)-1,3,4-oxadiazole-2(3H)-thione 6c. Yield: 81 %, m.p: 116–119 °C.: ¹H NMR (400 MHz, DMSO-*d*₆) δ: 2.40 (m, 1H, piperazine), 2.46 (m, 1H, piperazine), 2.64 (m, 1H, piperazine), 2.84 (m, 1H, piperazine), 3.51 (m, 1H, piperazine), 3.53 (m, 1H, piperazine), 3.57 (m, 1H, CH-piperazine), 3.72 (d, $J = 13.8$ Hz, 3H, CH₂Ph, CH₂Ph), 3.88 (m, 1H, CH₂Ph), 7.28 (dd, $J = 8.4$ Hz, $J = 3.2$ Hz, 4H, Ar), 7.35 (d, $J = 8.4$ Hz, 4H, Ar). ¹³C NMR (100 MHz, DMSO-*d*₆) δ: 178.2, 162.6, 137.4, 136.9, 132.1, 132.0, 131.0 (2C), 130.8 (2C), 128.7 (2C), 128.6 (2C), 60.7, 58.0, 56.5, 55.1, 52.5, 48.9. **Anal.** Calc. for C₂₀H₂₀Cl₂N₄OS (435.37): C, 55.17; H, 4.63; N, 12.87; S, 7.36. Found: C, 55.40; H, 4.74; N, 13.04; S, 7.38.

4.1.4.4. 5-(1,4-Bis(4-fluorobenzyl) piperazin-2-yl)-1,3,4-oxadiazole-2(3H)-thione 6d. Yield: 83 %, m.p: 103–105 °C. ¹H NMR (400 MHz, DMSO-*d*₆) δ: 2.42 (m, 1H, piperazine), 2.69 (m, 2H, piperazine), 2.85 (m, 1H, piperazine), 3.47–3.55 (m, 5H, CH₂Ph, CH-piperazine, piperazine), 3.72 (d, $J = 13.6$ Hz, 1H, CH₂Ph), 3.90 (m, 1H, CH₂Ph), 7.07–7.21 (t, $J_{H-F} = 8.4$ Hz, 4H, Ar), 7.24–7.37 (m, 4H, Ar). ¹³C NMR (100 MHz,

DMSO-*d*₆) δ: 178.1, 163.1, 162.6, 160.7, 134.4 (2C), 131.2, 131.2, 130.9, 130.8, 115.6, 115.5, 115.4, 115.3, 60.7, 58.0, 56.4, 55.0, 52.4, 48.7. **Anal.** Calc. for C₂₀H₂₀F₂N₄OS (402.46): C, 59.69; H, 5.01; N, 13.92; S, 7.97. Found: C, 59.87; H, 5.23; N, 14.15; S, 8.05.

4.1.4.5. 5-(1,4-Bis(4-methoxybenzyl) piperazin-2-yl)-1,3,4-oxadiazole-2(3H)-thione 6e. Yield: 86 %; m. p 135–137 °C. IR ν_{\max} , cm⁻¹: 3416 (NH), 1612 (C=N), 1511(C=S), 1406, 1181(C=N), 1302(C=O), 1244 (C=O), 1115 (N=N). ¹H NMR (400 MHz, DMSO-*d*₆) δ: 2.68 (m, 1H, piperazine), 2.77 (m, 2H, piperazine), 2.84–2.96 (m, 3H, piperazine), 3.57 (m, 1H, CH-piperazine), 3.66 (d, $J = 13.6$ Hz, 1H, CH₂Ph), 3.73 (s, 3H, OCH₃), 3.75 (s, 3H, OCH₃), 3.79 (m, 2H, CH₂Ph), 3.98 (m, 1H, CH₂Ph), 6.87 (d, $J = 8.8$ Hz, 2H, Ar), 6.92 (d, $J = 8.8$ Hz, 2H, Ar), 7.16 (d, $J = 8.8$ Hz, 2H, Ar), 7.29 (d, $J = 8.8$ Hz, 2H, Ar). ¹³C NMR (100 MHz, DMSO-*d*₆) δ: 178.3, 159.6, 159.0 (2C), 131.8 (2C), 130.4 (2C), 129.4 (2C), 114.3 (2C), 114.1 (2C), 60.1 (2C), 57.9, 57.8, 55.6, 55.5, 51.6, 51.5. **Anal.** Calc. for C₂₂H₂₆N₄O₃S (426.53): C, 61.95; H, 6.14; N, 13.14; S, 7.52. Found: C, 61.73; H, 6.30; N, 13.35; S, 7.68. **MS:** [M]⁺: 426.26 (26.98 %); base peak: 114.12(100 %).

4.1.4.6. 5-(1,4-Bis(3,4-dimethoxybenzyl)piperazin-2-yl)-1,3,4-oxadiazole-2(3H)-thione 6f. Yield: 74 %; m. p 164–166 °C. IR ν_{\max} , cm⁻¹: 3430 (NH), 1592 (C=N), 1516 (C=S), 1463, 1143 (C=N), 1373(C=O), 1266 (C=O), 1027 (N=N). ¹H NMR (400 MHz, DMSO-*d*₆) δ: 2.39 (m, 1H, piperazine), 2.62 (m, 2H, piperazine), 2.85 (m, 1H, piperazine), 3.42 (d, $J = 12.8$ Hz, 3H, piperazine), 3.52 (d, $J = 13.8$ Hz, 1H, CH₂Ph), 3.61 (d, $J = 13.6$ Hz, 1H, CH₂Ph), 3.71 (s, 9H, OCH₃), 3.73 (s, 3H, OCH₃), 3.81 (m, 2H, CH₂Ph), 6.72–6.81 (m, 2H, Ar), 6.82–6.90 (m, 4H, Ar). ¹³C NMR (100 MHz, DMSO-*d*₆) δ: 178.4, 162.7, 149.1, 149.0, 148.5, 148.4, 130.3, 129.6, 121.5, 121.2, 112.8, 112.7, 112.0, 111.9, 61.4, 58.5, 56.0, 55.9, 55.9 (2C), 54.8, 52.5, 49.1, 48.5. **Anal.** Calc. for C₂₄H₃₀N₄O₅S (486.58): C, 59.24; H, 6.21; N, 11.51; S, 6.59. Found: C, 59.51; H, 6.45; N, 11.78; S, 6.62.

4.1.4.7. 5-(1,4-Bis(4-dimethylaminobenzyl)piperazin-2-yl)-1,3,4-oxadiazole-2(3H)-thione 6g. Yield: 71 %; m. p: 89–91 °C. ¹H NMR (400 MHz, DMSO-*d*₆) δ: 2.33 (m, 1H, piperazine), 2.45 (m, 1H, piperazine), 2.61 (m, 2H, piperazine), 2.71 (m, 1H, piperazine), 2.80 (m, 2H, piperazine), 2.87 (s, 12H, 4 × CH₃), 3.52 (m, 2H, CH₂Ph), 3.56 (d, $J = 12.8$ Hz, 1H, CH₂Ph), 3.75 (m, 1H, CH₂Ph), 6.62–6.71 (d, $J = 0.8$ Hz, 4H, Ar), 7.00–7.16 (m, 4H, Ar). ¹³C NMR (100 MHz, DMSO-*d*₆) δ: 178.9, 162.4, 150.3, 150.2, 130.5 (2), 130.2 (2C), 124.8, 123.7, 112.6 (2C), 112.5 (2C), 61.2, 58.2, 56.2, 55.0, 52.2, 48.7, 40.7 (4C). **Anal.** Calc. for C₂₄H₃₂N₆OS (452.62): C, 63.69; H, 7.13; N, 18.57; S, 7.08. Found: C, 63.42; H, 7.40; N, 18.80; S, 6.97.

4.1.5. 1,4-Bis (un/substituted benzyl)-N-hydroxypiperazine-2-carboxamide 7a-f

Ethyl chloroformate (0.2 mL, 2 mmol) was added dropwise to a cooled (0–5 °C) stirred suspension of the respective piperazine-2-carboxylic acid, **4a-g**, (2 mmol) and triethylamine (0.6 mL, 4 mmol) in CH₂Cl₂ (10 mL). The reaction mixture was stirred for 1 h at (0–5 °C), then NH₂OH.HCl (0.3 g, 10 mmol) was added portion-wise and stirring continued at room temperature overnight. The organic layer was washed with water (3 × 25 mL) and dried over anhydrous MgSO₄, filtered off, and evaporated under reduced pressure. Recrystallization from ether afforded the targeted hydroxamic acids.

4.1.5.1. 1,4-Dibenzyl-N-hydroxypiperazine-2-carboxamide 7a. Yield: 69 %, m.p: 94–96 °C. ¹H NMR (400 MHz, DMSO-*d*₆) δ: 2.19–2.49 (m, 3H, piperazine), 2.62 (m, 2H, piperazine), 2.93 (m, 1H, piperazine), 3.24 (m, 1H, CH-piperazine), 3.40–3.75 (m, 3H, CH₂Ph, CH₂Ph), 3.91 (d, $J = 13.6$ Hz, 1H, CH₂Ph), 7.23–7.56 (m, 10H, Ar), 7.75 (br. s, 1H, OH, exchangeable), 11.66 (br. s, 1H, NH, exchangeable). ¹³C NMR (100 MHz, DMSO-*d*₆) δ: 172.8, 145.8 (2C), 138.2, 137.6, 130.1, 129.4 (2C),

129.1, 128.7 (2C), 127.6, 127.5, 62.6, 61.8, 58.9, 55.2, 52.5, 48.2. **Anal.** Calc. for $C_{20}H_{25}N_3O_2$ (339.43): C, 70.13; H, 7.12; N, 12.91. Found: C, 70.29; H, 7.25; N, 13.13.

4.1.5.2. *1,4-Bis(2-chlorobenzyl)-N-hydroxypiperazine-2-carboxamide 7b.* Yield: 74 %, m.p.: 151–153 °C. 1H NMR (400 MHz, DMSO- d_6) δ : 3.07 (m, 1H, piperazine), 3.46 (m, 6H, piperazine), 4.34 (s, 4H, 2 \times CH_2Ph), 7.38 (br. s, 1H, OH), 7.45–7.85 (m, 8H, Ar), 9.89 (br. s, 1H, NH, exchangeable). ^{13}C NMR (100 MHz, DMSO- d_6) δ : 173.4, 136.8, 135.8, 133.7, 133.6, 131.2, 130.8, 129.7, 129.6, 129.1, 128.9, 127.5, 127.4, 62.3, 58.8, 56.1, 55.8, 53.1, 47.9. **Anal.** Calc. for $C_{19}H_{21}Cl_2N_3O_2$ (394.29): C, 57.88; H, 5.37; N, 10.66. Found: C, 58.12; H, 5.50; N, 10.87.

4.1.5.3. *1,4-Bis(4-chlorobenzyl)-N-hydroxypiperazine-2-carboxamide 7c.* Yield: 70 %, m.p.: 98–100 °C. 1H NMR (400 MHz, DMSO- d_6) δ : 2.67 (m, 1H, piperazine), 3.04–3.13 (m, 6H, piperazine), 4.19 (s, 4H, 2 \times CH_2Ph), 7.38 (br. s, 1H, OH), 7.50–7.70 (m, 8H, Ar), 9.58 (br. s, 1H, NH). ^{13}C NMR (100 MHz, DMSO- d_6) δ : 172.8, 137.6, 136.2, 132.4, 132.1, 131.3(2C), 131.0(2C), 128.7(2C), 128.6(2C), 62.3, 60.7, 58.1, 54.9, 52.4, 47.8. **Anal.** Calc. for $C_{19}H_{21}Cl_2N_3O_2$ (394.29): C, 57.88; H, 5.37; N, 10.66. Found: C, 58.09; H, 5.53; N, 10.92.

4.1.5.4. *1,4-Bis(4-fluorobenzyl)-N-hydroxypiperazine-2-carboxamide 7d.* Yield: 62 %, m.p.: 159–161 °C. 1H NMR (400 MHz, DMSO- d_6) δ : 2.20–2.46 (m, 3H, piperazine), 2.61 (m, 2H, piperazine), 2.90 (m, 1H, piperazine), 3.23 (m, 1H, CH -piperazine), 3.56 (d, $J = 12$ Hz, 2H, CH_2Ph), 3.86 (d, $J = 13.2$ Hz, 1H, CH_2Ph), 4.04 (m, 1H, CH_2Ph), 7.06–7.24 (t, $J_{H-F} = 8$ Hz, 4H, Ar), 7.25–7.42 (m, 4H, Ar), 7.74 (br. s, 1H, OH, exchangeable). ^{13}C NMR (100 MHz, DMSO- d_6) δ : 172.9, 163.0, 160.6, 134.7, 134.0, 131.2, 131.1 (2C), 131.0, 115.5 (2C), 115.3 (2C), 62.5, 60.9, 58.1, 55.2, 52.5, 48.1. **Anal.** Calc. for $C_{19}H_{21}F_2N_3O_2$ (361.39): C, 63.15; H, 5.86; N, 11.63. Found: C, 63.23; H, 6.03; N, 11.81.

4.1.5.5. *1,4-Bis(4-methoxybenzyl)-N-hydroxypiperazine-2-carboxamide 7e.* Yield: 69 %, m.p.: 118–120 °C. 1H NMR (400 MHz, DMSO- d_6) δ : 2.03 (m, 2H, piperazine), 2.18 (m, 1H, piperazine), 2.54–2.65 (m, 3H, piperazine), 2.79 (m, 1H, CH -piperazine), 3.02 (d, $J = 13.2$ Hz, 1H, CH_2Ph), 3.32 (d, $J = 12.8$ Hz, 1H, CH_2Ph), 3.44 (d, $J = 12.8$ Hz, 1H, CH_2Ph), 3.68 (d, $J = 12.8$ Hz, 1H, CH_2Ph), 3.73 (s, 6H, 2 \times OCH_3), 6.87 (dd, $J = 8.4$ Hz, 2 Hz, 4H, Ar), 7.17 (d, $J = 8.4$ Hz, 2H, Ar), 7.22 (d, $J = 8.4$ Hz, 2H, Ar), 7.74 (br. s, 1H, OH), 8.84 (br. s, 1H, NH, exchangeable). ^{13}C NMR (100 MHz, DMSO- d_6) δ : 168.2, 158.8, 158.7, 130.6 (2C), 130.5 (2C), 130.1, 129.9, 114.0 (2C), 113.9 (2C), 64.5, 61.6, 58.5, 55.8, 55.5 (2C), 52.5, 50.3. **Anal.** Calc. for $C_{21}H_{27}N_3O_4$ (385.46): C, 65.44; H, 7.06; N, 10.90. Found: C, 65.71; H, 7.23; N, 11.09.

4.1.5.6. *1,4-Bis(3,4-dimethoxybenzyl)-N-hydroxypiperazine-2-carboxamide 7f.* Yield: 73 %, m.p.: 91–93 °C. 1H NMR (DMSO- d_6) δ : 2.71 (m, 1H, piperazine), 2.95 (m, 1H, piperazine), 3.29 (m, 3H, piperazine), 3.48 (m, 2H, CH -piperazine, piperazine), 3.75 (s, 12H, 4 \times OCH_3), 3.90–4.35 (m, 4H, 2 \times CH_2Ph), 6.62–7.16 (m, 6H, Ar), 7.32 (br. s, 1H, OH). ^{13}C NMR (100 MHz, DMSO- d_6) δ : 175.4, 149.6, 149.1 (2C), 148.6, 124.8, 123.2, 123.0, 121.7, 114.1, 113.2, 112.3, 112.0, 61.3, 58.4, 56.3, 56.0 (4C), 52.0, 50.7, 43.2. **Anal.** Calc. for $C_{23}H_{31}N_3O_6$ (445.51): C, 62.01; H, 7.01; N, 9.43. Found: C, 62.25; H, 7.19; N, 9.66.

4.1.6. 1,4-Dibenzylpiperazine-2-carboxamides 8a-s

Ethyl chloroformate (0.2 mL, 2 mmol) was added dropwise to a cooled (0–5 °C) stirred suspension of respective piperazine-2-carboxylic acid derivative, **4a-g**, (2 mmol) and triethylamine (0.6 mL, 4 mmol), in CH_2Cl_2 (10 mL). The reaction mixture was stirred for 1 h at (0–5 °C), then the proper amine (10 mmol) was added and stirring continued at room temperature overnight. The reaction mixture was washed with water (2 \times 25 mL), and the organic layer dried over anhydrous $MgSO_4$, filtered, and evaporated under reduced pressure. The product was

purified by column chromatography, gradient elution of CH_2Cl_2 : CH_3OH . The pure product, isolated at 1–5 % methanol.

4.1.6.1. *1,4-Dibenzyl-N-ethylpiperazine-2-carboxamide 8a.* Yield: 70 %, yellow oil. 1H NMR (400 MHz, DMSO- d_6) δ : 0.99 (t, $J = 7.2$ Hz, 3H, CH_2CH_3), 1.23 (m, 1H, piperazine), 2.11 (d, $J = 8.4$ Hz, 1H, piperazine), 2.17 (d, $J = 10.4$ Hz, 1H, piperazine), 2.61 (m, 1H, piperazine), 2.69 (m, 1H, piperazine), 2.83 (m, 1H, piperazine), 3.05 (m, 2H, CH_2Ph , CH -piperazine), 3.18 (m, 2H, CH_2CH_3), 3.41 (d, $J = 13.6$ Hz, 1H, CH_2Ph), 3.49 (d, $J = 13.6$ Hz, 1H, CH_2Ph), 3.71 (d, $J = 13.2$ Hz, 1H, CH_2Ph), 7.20–7.36 (m, 10H, Ar), 7.90 (t, $J = 5.6$ Hz, 1H, NH, exchangeable). ^{13}C NMR (100 MHz, DMSO- d_6) δ : 170.6, 137.8, 137.7, 129.0 (2C), 128.8 (2C), 128.2 (2C), 128.1 (2C), 127.0 (2C), 66.4, 61.8, 59.0, 55.6, 52.1, 49.8, 33.2, 14.8. **Anal.** Calc. for $C_{21}H_{27}N_3O$ (337.46): C, 74.74; H, 8.06; N, 12.45. Found: C, 74.95; H, 8.23; N, 12.71.

4.1.6.2. *1,4-Dibenzyl-N-phenylpiperazine-2-carboxamide 8b.* Yield: 74 %, m.p.: 100–101 °C. 1H NMR (400 MHz, DMSO- d_6) δ : 2.36 (m, 2H, piperazine), 2.62 (m, 1H, piperazine), 2.79 (m, 1H, piperazine), 3.14 (m, 1H, piperazine), 3.30 (m, 2H, piperazine), 3.52 (m, 3H, CH_2Ph , CH_2Ph), 3.80 (m, 1H, CH_2Ph), 7.05 (t, $J = 7.6$ Hz, 1H, Ar), 7.24–7.37 (m, 12H, Ar), 7.63 (dd, $J = 8$ Hz, $J = 1.2$ Hz, 2H, Ar), 9.95 (br. s, 1H, NH, exchangeable). ^{13}C NMR (100 MHz, DMSO- d_6) δ : 170.2, 139.0 (2C), 138.2, 129.4 (2C), 129.1 (2C), 129.0 (2C), 128.7 (2C), 128.6 (2C), 127.6, 127.4, 124.0, 120.1 (2C), 66.7, 62.1, 59.4, 55.5, 52.4, 50.0. **Anal.** Calc. for $C_{25}H_{27}N_3O$ (385.5): C, 77.89; H, 7.06; N, 10.90. Found: C, 77.71; H, 7.28; N, 11.14.

4.1.6.3. *1,4-Dibenzyl-N-(4-nitrophenyl) piperazine-2-carboxamide 8c.* Yield: 72 %, yellow oil. 1H NMR (400 MHz, DMSO- d_6) δ : 2.33 (m, 2H, piperazine), 2.41 (m, 1H, piperazine), 2.72 (m, 1H, piperazine), 3.00 (m, 1H, piperazine), 3.24 (m, 1H, piperazine), 3.35 (d, $J = 14$ Hz, 2H, CH_2Ph , CH -piperazine), 3.53 (d, $J = 13.2$ Hz, 1H, CH_2Ph), 3.62 (d, $J = 11.2$ Hz, 1H, CH_2Ph), 3.84 (d, $J = 13.2$ Hz, 1H, CH_2Ph), 7.15–7.40 (m, 15H, Ar, NH). ^{13}C NMR (100 MHz, DMSO- d_6) δ : 171.7, 139.0 (2C), 138.5, 138.4, 129.1 (2C), 129.0 (2C), 128.9, 128.7, 128.6 (2C), 128.5 (2C), 128.0, 127.7, 127.4 (2C), 62.1, 61.3, 60.2, 59.0, 55.4, 53.3. **Anal.** Calc. for $C_{25}H_{26}N_4O_3$ (430.5): C, 69.75; H, 6.09; N, 13.01. Found: C, 69.94; H, 6.23; N, 13.27. **MS:** $[M]^+$: 430 (1 %), base peak: 91.1 (100 %).

4.1.6.4. *1,4-Dibenzyl-N-(4-methoxyphenyl) piperazine-2-carboxamide 8d.* Yield: 67 %, m.p.: 109–111 °C. 1H NMR (400 MHz, DMSO- d_6) δ : 2.23 (m, 2H, piperazine), 2.40 (t, $J = 10$ Hz, 1H, piperazine), 2.63 (m, 1H, piperazine), 2.78 (t, $J = 12.8$ Hz, 2H, piperazine), 3.11 (m, 1H, CH -piperazine), 3.28 (d, $J = 13.4$ Hz, 1H, CH_2Ph), 3.50 (m, 2H, CH_2Ph), 3.72 (s, 3H, OCH_3), 3.79 (d, $J = 13.2$ Hz, 1H, CH_2Ph), 6.88 (d, $J = 8.4$ Hz, 2H, Ar), 7.23–7.39 (m, 10H, Ar), 7.56 (d, $J = 8$ Hz, 2H, Ar), 9.81 (br. s, 1H, NH, exchangeable). ^{13}C NMR (100 MHz, DMSO- d_6) δ : 169.8, 155.9, 138.3, 138.2, 132.1, 129.4 (2C), 129.3 (2C), 128.7 (2C), 128.6 (2C), 127.5 (2C), 121.7 (2C), 114.3 (2C), 66.8, 62.2, 59.5, 55.7, 55.6, 52.5, 50.2. **Anal.** Calc. for $C_{26}H_{29}N_3O_2$ (415.53): C, 75.15; H, 7.03; N, 10.11. Found: C, 74.97; H, 7.26; N, 10.39.

4.1.6.5. *1,4-Dibenzyl-N-(pyridin-4-yl) piperazine-2-carboxamide 8e.* Yield: 73 %, m.p.: 129–131 °C. 1H NMR (400 MHz, DMSO- d_6) δ : 2.27 (m, 2H, piperazine), 2.44 (m, 1H, piperazine), 2.75 (d, $J = 12$ Hz, 1H, piperazine), 2.84 (m, 1H, piperazine), 2.99 (m, 1H, piperazine), 3.18 (m, 1H, CH -piperazine), 3.31 (m, 1H, CH_2Ph), 3.50 (m, 2H, CH_2Ph), 3.76 (d, $J = 13.2$ Hz, 1H, CH_2Ph), 7.21–7.36 (m, 10H, Ar), 7.62 (d, $J = 5.6$ Hz, 2H, pyridine), 8.24 (d, $J = 6$ Hz, 2H, pyridine), 10.30 (br. s, 1H, NH, exchangeable). ^{13}C NMR (100 MHz, DMSO- d_6) δ : 171.7, 150.8 (2C), 145.7, 138.2, 138.1, 129.4 (2C), 129.3 (2C), 128.7 (2C), 128.6 (2C), 127.6, 127.5, 114.0 (2C), 66.4, 62.1, 59.5, 55.4, 52.4, 49.9. **Anal.** Calc. for $C_{24}H_{26}N_4O$ (386.49): C, 74.58; H, 6.78; N, 14.50. Found: C, 74.32; H, 6.85; N, 14.76.

4.1.6.6. *1,4-Dibenzyl-N-cyclohexylpiperazine-2-carboxamide 8f*. Yield: 72 %, m.p: 89–92 °C. ^1H NMR (400 MHz, DMSO- d_6) δ : 1.17–1.28 (m, 4H, cyclohexane), 1.55 (m, 1H, cyclohexane), 1.57–1.77 (m, 5H, cyclohexane), 2.10–2.26 (m, 3H, piperazine), 2.58 (d, $J = 10.8$ Hz, 1H, piperazine), 2.66 (t, $J = 9.6$ Hz, 2H, piperazine), 2.87 (dd, $J = 8.8$ Hz, $J = 2.8$ Hz, 1H, cyclohexane), 3.17 (d, $J = 13.6$ Hz, 1H, CH-piperazine), 3.45 (m, 2H, CH₂Ph), 3.57 (m, 1H, CH₂Ph), 3.71 (d, $J = 13.6$ Hz, 1H, CH₂Ph), 7.22–7.35 (m, 10H, Ar), 7.69 (d, $J = 8.4$ Hz, NH, exchangeable). ^{13}C NMR (100 MHz, DMSO- d_6) δ : 170.2, 138.3 (2C), 129.4 (2C), 129.3 (2C), 128.7 (2C), 128.6 (2C), 127.5 (2C), 66.3, 62.2, 59.4, 56.0, 52.6, 50.2, 47.7, 32.7 (2C), 25.6, 25.0. **Anal.** Calc. for C₂₅H₃₃N₃O (391.55): C, 76.69; H, 8.49; N, 10.73. Found: C, 76.48; H, 8.65; N, 10.98.

4.1.6.7. *1,4-Bis(2-chlorobenzyl)-N-ethylpiperazine-2-carboxamide 8g*. Yield: 67 %, oil. ^1H NMR (400 MHz, DMSO- d_6) δ : 0.96 (t, $J = 7.2$ Hz, 3H, CH₂CH₃), 2.29 (m, 2H, piperazine), 2.43 (m, 1H, piperazine), 2.59 (m, 1H, piperazine), 2.71 (m, 2H, piperazine), 3.01 (m, 1H, CH-piperazine), 3.10 (m, 2H, CH₂CH₃), 3.51 (d, $J = 13.8$ Hz, 1H, CH₂Ph), 3.55 (s, 2H, CH₂Ph), 3.67 (d, $J = 13.8$ Hz, 1H, CH₂Ph), 7.24–7.35 (m, 4H, Ar), 7.37–7.47 (m, 3H, Ar), 7.62 (dd, $J = 7.2$ Hz, 1.8 Hz, 1H, Ar), 7.91 (t, $J = 5.6$ Hz, 1H, NH, exchangeable). ^{13}C NMR (100 MHz, DMSO- d_6) δ : 170.6, 135.9, 135.7, 133.9, 133.5, 131.5, 131.4, 129.8, 129.6, 129.3, 129.1, 127.5, 127.4, 58.9, 56.0, 55.7, 55.4, 52.6, 50.1, 33.6, 15.2. **Anal.** Calc. for C₂₁H₂₅Cl₂N₃O (406.35): C, 62.07; H, 6.20; N, 10.34. Found: C, 61.89; N, 6.43; Cl, 10.51.

4.1.6.8. *1,4-Bis(2-chlorobenzyl)-N-phenylpiperazine-2-carboxamide 8h*. Yield: 78 %, orange oil. ^1H NMR (400 MHz, DMSO- d_6) δ : 2.36 (m, 1H, piperazine), 2.37 (m, 1H, piperazine), 2.55 (d, $J = 12$ Hz, 2H, piperazine), 2.89 (m, 1H, piperazine), 3.04 (m, 1H, piperazine), 3.57 (s, 3H, CH₂Ph, CH-piperazine), 3.75 (d, $J = 14$ Hz, 1H, CH₂Ph), 3.95 (d, $J = 14$ Hz, 1H, CH₂Ph), 7.23–7.35 (m, 6H, Ar), 7.41 (t, $J = 7.6$ Hz, 3H, Ar), 7.48 (d, $J = 7.2$ Hz, 2H, Ar), 7.53 (d, $J = 7.6$ Hz, 2H, Ar), 9.98 (br. s, 1H, NH, exchangeable). ^{13}C NMR (100 MHz, DMSO- d_6) δ : 173.7, 136.8 (2C), 135.8, 133.7, 133.5, 131.1 (2C), 130.8, 129.7 (2C), 129.6, 129.1 (2C), 128.9 (2C), 127.5, 127.4 (2C), 58.8, 56.1, 55.9, 53.2, 49.1, 47.9. **Anal.** Calc. for C₂₅H₂₅Cl₂N₃O (454.39): C, 66.08; H, 5.55; N, 9.25. Found: C, 66.29; H, 5.43; N, 9.51. **MS:** [M]⁺: 454.95(14.51 %); M⁺¹: 455.98(9.10 %); base peak: 433.05 (100 %).

4.1.6.9. *1,4-Bis(2-chlorobenzyl)-N-cyclohexylpiperazine-2-carboxamide 8i*. Yield: 81 %, m.p: 158–159 °C. ^1H NMR (400 MHz, DMSO- d_6) δ : 1.24 (m, 2H, cyclohexane), 1.38–1.86 (m, 8H, cyclohexane), 2.35 (m, 2H, piperazine), 2.59 (m, 1H, piperazine), 2.74 (m, 2H, piperazine), 3.06 (m, 1H, piperazine), 3.28 (m, 1H, cyclohexane), 3.49–3.63 (m, 4H, CH₂Ph, CH₂Ph, CH-piperazine), 3.70 (d, $J = 14$ Hz, 1H, CH₂Ph), 7.26–7.51 (m, 7H, Ar), 7.61 (d, $J = 7.2$ Hz, 1H, Ar), 7.69 (br. s, 1H, NH, exchangeable). ^{13}C NMR (100 MHz, DMSO- d_6) δ : 169.7, 136.0, 135.7, 133.9, 133.5, 131.6, 131.3, 129.8, 129.7, 129.3, 129.2, 127.6, 127.5, 65.6, 58.8, 55.9, 55.5, 52.5, 50.0, 47.7, 33.8, 32.7, 25.8, 25.6, 24.9. **Anal.** Calc. for C₂₅H₃₁Cl₂N₃O (460.44): C, 65.21; H, 6.79; N, 9.13. Found: C, 64.98; H, 7.01; N, 9.40.

4.1.6.10. *1,4-Bis(4-chlorobenzyl)-N-ethylpiperazine-2-carboxamide 8j*. Yield: 75 %, m.p: 131–132 °C. IR ν_{max} cm⁻¹: 3418 (NH-amide), 1674 (C=O), 1491(C–N), 1091(C–N). ^1H NMR (400 MHz, DMSO- d_6) δ : 0.99 (t, $J = 7.2$ Hz, 3H, CH₂CH₃), 2.12 (d, $J = 11.2$ Hz, 2H, piperazine), 2.19 (m, 1H, piperazine), 2.58 (d, $J = 11.8$ Hz, 1H, piperazine), 2.62 (d, $J = 12$ Hz, 1H, piperazine), 2.69 (d, $J = 12.8$ Hz, 1H, piperazine), 2.87 (m, 1H, CH-piperazine), 3.06 (m, 1H, CH₂Ph), 3.16 (m, 2H, CH₂CH₃), 3.45 (s, 2H, CH₂Ph), 3.69 (d, $J = 13.2$ Hz, 1H, CH₂Ph), 7.29 (d, $J = 7.2$ Hz, 2H, Ar), 7.35 (m, 1H, Ar), 7.37 (m, 5H, Ar), 7.94 (t, $J = 5.6$ Hz, 1H, NH, exchangeable). ^{13}C NMR (100 MHz, DMSO- d_6) δ : 170.9, 137.3, 137.3, 132.1, 132.0, 131.3 (2C), 131.1 (2C), 128.6 (2C), 128.5 (2C), 66.6, 61.2, 58.5, 55.9, 52.4, 50.3, 33.7, 15.3. **Anal.** Calc. for C₂₁H₂₅Cl₂N₃O

(406.35): C, 62.07; H, 6.20; N, 10.34. Found: C, 61.88; H, 6.34; N, 10.56.

4.1.6.11. *1,4-Bis(4-chlorobenzyl)-N-phenylpiperazine-2-carboxamide 8k*. Yield: 78 %, m.p: 63–64 °C. IR ν_{max} cm⁻¹: 3324 (NH-amide), 1682 (C=O), 1145 (C–N), 1175 (C–N). ^1H NMR (400 MHz, DMSO- d_6) δ : 2.22 (m, 2H, piperazine), 2.40 (m, 1H, piperazine), 2.56 (m, 1H, piperazine), 2.74 (d, $J = 9.6$ Hz, 2H, piperazine), 3.18 (m, 1H, CH-piperazine), 3.28 (d, $J = 14$ Hz, 2H, CH₂Ph), 3.48 (m, 1H, CH₂Ph), 3.71 (d, $J = 14$ Hz, 1H, CH₂Ph), 7.03 (t, $J = 7.6$ Hz, 1H, Ar), 7.25–7.39 (m, 10H, Ar), 7.62 (d, $J = 8$ Hz, 2H, Ar), 10.02 (br. s, 1H, NH, exchangeable). ^{13}C NMR (100 MHz, DMSO- d_6) δ : 170.3, 139.0, 137.5, 137.2, 132.0 (2C), 131.2 (2C), 131.1 (2C), 129.1 (2C), 128.6 (2C), 128.5 (2C), 124.0, 120.1 (2C), 66.3, 61.1, 58.5, 55.5, 52.3, 50.0. **Anal.** Calc. for C₂₅H₂₅Cl₂N₃O (454.39): C, 66.08; H, 5.55; N, 9.25. Found: C, 66.24; H, 5.38; N, 9.43.

4.1.6.12. *1,4-Bis(4-fluorobenzyl)-N-ethylpiperazine-2-carboxamide 8l*. Yield: 71 %, m.p: 124–127 °C. IR ν_{max} cm⁻¹: 3366 (NH-amide), 1663 (C=O), 1223 (C–N), 1173 (C–N). ^1H NMR (400 MHz, DMSO- d_6) δ : 0.98 (t, $J = 7.2$ Hz, 3H, CH₂CH₃), 1.95–2.27 (m, 3H, piperazine), 2.55–2.75 (m, 3H, piperazine), 2.83 (m, 1H, CH-piperazine), 3.13 (m, 2H, CH₂CH₃), 3.43 (m, 3H, CH₂Ph, CH₂Ph), 3.68 (d, $J = 12.8$ Hz, 1H, CH₂Ph), 7.06–7.17 (t, $J_{\text{H-F}} = 8$ Hz, 4H, Ar), 7.27–7.41 (m, 4H, Ar), 7.92 (br. s, 1H, NH, exchangeable). ^{13}C NMR (100 MHz, DMSO- d_6) δ : 171.0, 163.0, 160.6, 134.4, 134.3, 131.4, 131.3, 131.2, 131.1, 115.5, 115.4, 115.3, 115.2, 66.8, 61.2, 58.6, 55.9, 52.5, 50.2, 33.6, 15.3. **Anal.** Calc. for C₂₁H₂₅F₂N₃O (373.44): C, 67.54; H, 6.75; N, 11.25. Found: C, 67.37; H, 6.90; N, 11.25. **MS:** [M]⁺: 373.4(60 %); base peak: 109.1 (100 %).

4.1.6.13. *1,4-Bis(4-fluorobenzyl)-N-phenylpiperazine-2-carboxamide 8m*. Yield: 77 %, m.p: 59–61 °C. ^1H NMR (400 MHz, DMSO- d_6) δ : 2.31 (m, 2H, piperazine), 2.41 (m, 1H, piperazine), 2.71 (m, 1H, piperazine), 2.97 (m, 1H, piperazine), 3.52 (d, $J = 13.6$ Hz, 1H, piperazine), 3.60 (d, $J = 12.4$ Hz, 1H, CH-piperazine), 3.82 (d, $J = 13.6$ Hz, 1H, CH₂Ph), 4.08 (m, 3H, CH₂Ph, CH₂Ph), 7.08–7.16 (t, $J_{\text{H-F}} = 8.4$ Hz, 6H, Ar), 7.25–7.35 (m, 7H, Ar). ^{13}C NMR (100 MHz, DMSO- d_6) δ : 171.6, 162.9, 160.5, 136.2, 134.6 (2C), 130.9 (2C), 130.8 (2C), 130.7 (2C), 130.6, 115.4 (2C), 115.3 (2C), 115.2, 115.1, 62.1, 61.1, 60.3, 58.2, 55.3, 53.2. **Anal.** Calc. for C₂₅H₂₅F₂N₃O (421.48): C, 71.24; H, 5.98; N, 9.97. Found: 70.97; H, 6.09; N, 10.21.

4.1.6.14. *1,4-Bis(4-fluorobenzyl)-N-(pyridin-4-yl) piperazine-2-carboxamide 8n*. Yield: 72 %, m.p: 177–179 °C. ^1H NMR (400 MHz, DMSO- d_6) δ : 2.26 (m, 2H, piperazine), 2.44 (m, 1H, piperazine), 2.58 (m, 1H, piperazine), 2.79 (m, 2H, piperazine), 3.18 (m, 1H, CH-piperazine), 3.32 (d, $J = 13.6$ Hz, 2H, CH₂Ph), 3.49 (m, 1H, CH₂Ph), 3.73 (d, $J = 13.6$ Hz, 1H, CH₂Ph), 7.06–7.16 (m, 4H, Ar), 7.31 (td, $J_{\text{H-F}} = 6.8$ Hz, $J = 2.4$ Hz, 2H, Ar), 7.37 (td, $J_{\text{H-F}} = 5.6$ Hz, $J = 2$ Hz, 2H, Ar), 7.63 (d, $J = 4.8$ Hz, 2H, pyridine), 8.43 (d, $J = 5$ Hz, 2H, pyridine), 10.32 (br. s, 1H, NH). ^{13}C NMR (100 MHz, DMSO- d_6) δ : 171.6, 163.0, 160.6, 150.7 (2C), 145.8, 134.4, 134.2, 131.2 (2C), 131.1 (2C), 115.5 (2C), 115.3 (2C), 114.0 (2C), 66.3, 61.1, 58.6, 55.2, 52.2, 49.8. **Anal.** Calc. for C₂₄H₂₄F₂N₄O (422.47): C, 68.23; H, 5.73; N, 13.26. Found: C, 68.41; H, 5.86; N, 13.42.

4.1.6.15. *1,4-Bis(4-fluorobenzyl)-N-cyclohexylpiperazine-2-carboxamide 8o*. Yield: 79 %, m.p: 139–141 °C. ^1H NMR (400 MHz, DMSO- d_6) δ : 1.11–1.30 (m, 6H, cyclohexane), 1.53 (d, $J = 12$ Hz, 1H, cyclohexane), 1.61–1.71 (m, 4H, piperazine, cyclohexane), 2.13 (m, 2H, piperazine), 2.22 (m, 1H, piperazine), 2.55 (m, 1H, piperazine), 2.64 (m, 2H, CH-cyclohexane, piperazine), 2.88 (m, 1H, CH-piperazine), 3.16 (d, $J = 12.8$ Hz, 1H, CH₂Ph), 3.57 (m, 2H, CH₂Ph), 3.67 (d, $J = 13.2$ Hz, 1H, CH₂Ph), 7.12 (td, $J_{\text{H-F}} = 2$ Hz, $J_{\text{H-F}} = 8.8$ Hz, 4H, Ar), 7.30 (m, 2H, Ar), 7.35 (m, 2H, Ar), 7.72 (d, $J = 8.4$ Hz, 1H, NH, exchangeable). ^{13}C NMR (100 MHz, DMSO- d_6) δ : 170.2, 163.0, 160.6, 134.4, 134.3, 131.3, 131.2,

131.1, 131.0, 115.5, 115.4, 115.2, 115.1, 66.2, 61.2, 58.4, 55.8, 52.4, 50.0, 47.8, 32.7 (2C), 25.6, 25.0 (2C). **Anal.** Calc. for $C_{25}H_{31}F_2N_3O$ (427.53): C, 70.23; H, 7.31; N, 9.83. Found: C, 70.09; H, 7.43; N, 10.08.

4.1.6.16. 1,4-Bis(4-methoxybenzyl)-N-ethylpiperazine-2-carboxamide 8p. Yield: 65 %, yellow oil. 1H NMR (400 MHz, DMSO- d_6) δ : 1.01 (t, J = 7.2, 3H, CH_2CH_3), 2.03–2.13 (m, 3H, piperazine), 2.58–2.71 (m, 3H, piperazine), 2.81 (m, 1H, CH -piperazine), 3.07 (m, 2H, CH_2CH_3), 3.18 (m, 1H, CH_2Ph), 3.43 (d, J = 12 Hz, 2H, CH_2Ph), 3.73 (d, J = 12 Hz, 1H, CH_2Ph), 3.76 (s, 6H, $2 \times OCH_3$), 6.87 (dd, J = 8 Hz, J = 1.6 Hz, 4H, Ar), 7.18 (d, J = 8 Hz, 2H, Ar), 7.25 (d, J = 8 Hz, 2H, Ar), 7.88 (t, J = 5.6 Hz, 1H, NH, exchangeable). ^{13}C NMR (100 MHz, DMSO- d_6) δ : 171.8, 158.8 (2C), 130.3 (4C), 114.4 (2C), 114.1 (2C), 114.0 (2C), 61.5, 60.2, 58.4, 55.5, 55.3, 53.1, 47.9, 29.1, 14.6. **Anal.** Calc. for $C_{23}H_{31}N_3O_3$ (397.51): C, 69.49; H, 7.86; N, 10.57. Found: C, 69.70; H, 8.02; N, 10.80.

4.1.6.17. 1,4-Bis(4-methoxybenzyl)-N-phenylpiperazine-2-carboxamide 8q. Yield: 72 %, m.p: 59–60 °C. 1H NMR (400 MHz, DMSO- d_6) δ : 2.32 (m, 2H, piperazine), 2.65 (m, 1H, piperazine), 2.95 (m, 1H, piperazine), 3.29 (d, J = 12.8 Hz, 1H, piperazine), 3.45 (d, J = 12.8 Hz, 1H, piperazine), 3.53 (m, 1H, CH -piperazine), 3.73 (s, 6H, $2 \times OCH_3$), 4.08 (m, 4H, $2 \times CH_2Ph$), 6.83–6.89 (dd, J = 8.8 Hz, J = 2 Hz, 6H, Ar), 7.11–7.23 (m, 7H, Ar). ^{13}C NMR (100 MHz, DMSO- d_6) δ : 171.8, 158.8 (2C), 130.7, 130.4 (2C), 130.3 (4C), 130.2 (2C), 114.2, 114.1 (3C), 114.0 (3C), 61.5, 60.2, 58.4, 55.5 (2C), 55.3, 53.1, 48.0. **Anal.** Calc. for $C_{27}H_{31}N_3O_3$ (445.55): C, 72.78; H, 7.01; N, 9.43. Found: C, 72.59; H, 7.21; N, 9.60.

4.1.6.18. 1,4-Bis(3,4-dimethoxybenzyl)-N-ethylpiperazine-2-carboxamide 8r. Yield: 71 %, m.p: 121–122 °C. IR ν_{max} cm^{-1} : 3336 (NH-amide), 1652 (C=O), 1264 (C–N), 1233 (C–N). 1H NMR (400 MHz, DMSO- d_6) δ : 1.01 (t, J = 7.2 Hz, 3H, CH_2CH_3), 2.12 (m, 3H, piperazine), 2.60 (m, 1H, piperazine), 2.68 (m, 2H, piperazine), 2.82 (m, 1H, CH -piperazine), 3.07 (m, 2H, CH_2CH_3), 3.19 (m, 1H, CH_2Ph), 3.37 (s, 1H, CH_2Ph), 3.39 (s, 1H, CH_2Ph), 3.65 (d, J = 13.2 Hz, 1H, CH_2Ph), 3.73 (s, 9H, $3 \times OCH_3$), 3.75 (s, 3H, OCH_3), 6.76–6.93 (m, 6H, Ar), 7.92 (t, J = 6 Hz, 1H, NH, exchangeable). ^{13}C NMR (100 MHz, DMSO- d_6) δ : 171.2, 149.1, 149.0, 148.4, 148.3, 130.6, 130.4, 121.7, 121.4, 113.4, 113.0, 112.0, 111.9, 66.6, 62.0, 59.2, 56.0, 55.9 (2C), 55.8, 55.7, 52.5, 50.2, 33.6, 15.3. **Anal.** Calc. for $C_{25}H_{35}N_3O_5$ (457.56): C, 65.62; H, 7.71; N, 9.18. Found: C, 65.89; H, 7.94; N, 9.40.

4.1.6.19. 1,4-Bis(3,4-dimethoxybenzyl)-N-phenylpiperazine-2-carboxamide 8s. Yield: 77 %, m.p: 66–68 °C. 1H NMR (400 MHz, DMSO- d_6) δ : 2.27 (m, 1H, piperazine), 2.42 (m, 1H, piperazine), 2.62 (m, 1H, piperazine), 2.76 (m, 1H, piperazine), 2.84 (m, 1H, piperazine), 3.10 (m, 1H, piperazine), 3.21 (m, 1H, CH -piperazine), 3.29 (m, 1H, CH_2Ph), 3.43 (m, 1H, CH_2Ph), 3.47 (m, 1H, CH_2Ph), 3.69 (s, 2H, OCH_3), 3.71 (s, 2H, OCH_3), 3.72 (s, 8H, $3 \times OCH_3$), 4.05 (m, 1H, CH_2Ph), 6.74–6.93 (m, 6H, Ar), 7.06 (t, J = 8 Hz, 1H, Ar), 7.30 (t, J = 7.2 Hz, 2H, Ar), 7.65 (dd, J = 8.8 Hz, J = 1.2 Hz, 2H, Ar), 9.95 (br. s, 1H, NH, exchangeable). ^{13}C NMR (100 MHz, DMSO- d_6) δ : 170.4, 149.1, 149.0, 148.4, 148.3, 139.1, 130.5, 130.4, 129.1 (2C), 123.9, 121.6, 121.5, 120.0 (2C), 113.1, 112.9, 112.0, 111.9, 62.0, 60.8, 59.2, 56.0, 55.9, 55.9, 55.8, 55.4, 52.4, 49.9. **Anal.** Calc. for $C_{29}H_{35}N_3O_5$ (505.61): C, 68.89; H, 6.98; N, 8.31. Found: C, 68.71; H, 7.15; N, 8.54.

4.2. Biochemical analyses

4.2.1. Cholinesterase inhibitory assay

Acetylthiocholine iodide (AChI) and butyrylthiocholine iodide (BChI) were used as substrates in the enzymatic reactions. Additionally, 5,5-dithio bis-(2-nitro-benzoic acid) (DTNB) was used as a detection reagent for finding the AChE and BChE activities. Briefly, 1 mL of Tris/HCl buffer (1.0 M, pH = 8) and 10 μ L of sample solution at different concentrations were dissolved in ultrapure water. Then, 50 mL

Electrophorus electricus AChE and *Equine* serum BChE solution were mixed and incubated at room temperature for 10 min. After the incubation period, 50 μ L of DTNB (0.5 mM) was added. Then, the reaction was allowed to start by the addition of 50 μ L of AChI (10 mM) or BChI. The breakdown of these substrates was watched spectrophotometrically by yellow color formation (λ = 412 nm) of 5-thio-2-nitrobenzoate anion as the result of the reaction of DTNB with thiocholine from hydrolysis of AChI or BChI. K_i values were calculated from Lineweaver – Burk curves.

4.2.2. Kinetic study

Kinetic characterization of AChE was conducted experimentally using Ellman's method [27,28] at three different concentrations of the inhibitor. A parallel experiment was conducted in the absence of the inhibitor. Lineweaver-Burk reciprocal plots were constructed by plotting 1/velocity against 1/[Substrate]. The K_i value is the dissociation constant that defines the binding affinity between the inhibitor and the enzyme. This value is obtained from Lineweaver-Burk reciprocal plots studied at three different inhibitor concentrations and recorded by taking the arithmetic average. Then the results were analyzed using Microsoft Office Excel 2013.

4.2.3. Cytotoxicity study

Reducing 3-(4,5-dimethyl-2-thiazolyl)-2,5-diphenyl-2H-tetrazolium bromide (MTT) to its insoluble formazan, about mitochondrial metabolic function, evaluated cell viability. Briefly, neuronal SH-SY5Y cells were seeded in a 96-well plate at 2×10^4 cells per well. Subsequently, SH-SY5Y cells were treated for 24 h with different concentrations of the studied compounds **4c** and **7b** (2.5 – 80 μ M). Then the treatment medium was replaced with MTT solution (0.5 mg/mL) in Hank's Balanced Salt Solution (HBSS) for 2 h at 37 °C in 5 % CO_2 . After washing with HBSS, formazan crystals were dissolved in isopropanol. The amount of formazan was measured (λ = 570 nm, reference filter 690 nm) using a multilabel plate reader (VICTOR™ X3, perkinelmer, Waltham, MA, USA) and an Anthos Zenyth 200rt microplate reader (Biochrom, UK). The cytotoxicity of the test compound was obtained using the following formula: $[(A - B)/A \times 100]$, where A is the absorbance of untreated cells and B the absorbance of cells treated with different concentrations of the test compounds. Cytotoxic concentrations for 50 % of cells were figured out by linear regression.

4.3. Molecular modeling studies

4.3.1. Molecular docking

The molecular docking studies were performed using molecular operating environment software (MOE 2020.01). X-ray crystallographic structure of recombinant hAChE complexed with donepezil (PDB code 4EY7) and that of hBChE complexed with tacrine (PDB code: 4BDS) are downloaded from RCSB's protein data bank. The docking protocol involves target preparation through the removal of water molecules except those in a water-mediated hydrogen bond with the co-crystallized ligands. Then, protons and partial charges were added to the protein structure. To guarantee the accuracy of the docking protocol, redocking of the co-crystallized ligands, (donepezil or tacrine, respectively) into the respective active site is performed. The docking validation results showed almost perfect alignment with the original ligand with rmsd of 0.5805 and displaying the same binding interactions. The ligands were protonated, and Molecular Force Field (MMFF94X) minimized energy to a gradient of 0.05. The docking of the most stable conformers was done using Triangle Matcher Replacement and London's dG scoring function.

4.3.2. Molecular dynamics simulation

The initial complexes of hAChE with compound **4c**, and that of hBChE with compound **7b** were taken from molecular docking results. The protein structure was first examined for missing hydrogens, then the protonation states of the amino acid residues were set (pH = 7.4) and the

co-crystalized water molecules were removed. The entire structure was placed in an orthorhombic box of TIP3P water having 0.15 M Na⁺ and Cl⁻ ions in a 20 Å solvent buffer. After that, the systems were energy-minimized and equilibrated for 50 ns. The top-scoring poses of compounds **4c** and **7b** were employed as a starting point for the simulation of protein–ligand complexes. The parameters and topologies of the compounds **4c** and **7b** were determined using the VMD plugin Force Field Toolkit (FFTK), derived with the CHARMM General Force Field (CGenFF) program v. 2.4.0 [42]. Finally, the generated parameters, and topology files were loaded to VMD to readily read the protein–ligand complexes. Binding Free Energy Calculations using Molecular Mechanics Poisson-Boltzmann Surface Area (MM-PBSA) embedded in the MMPBSA.py module of AMBER18, were performed to estimate the binding free energy of the docked complexes. A hundred frames were processed from the trajectories in total, and the system's net energy was estimated using the following equation:

$$\Delta G_{\text{Binding}} = \Delta G_{\text{Complex}} - \Delta G_{\text{Receptor}} - \Delta G_{\text{Inhibitor}}$$

Each of the terms requires calculating various energy components, including Van der Waals energy, electrostatic energy, molecular mechanics, internal energy, and polar contribution to solvation energy.

Declaration of Competing Interest

The authors declare that they have no known competing financial interests or personal relationships that could have appeared to influence the work reported in this paper.

Appendix A. Supplementary data

Supplementary data to this article can be found online at <https://doi.org/10.1016/j.bioorg.2023.106916>.

References

- C. Patterson, World Alzheimer Report 2018: The State of the Art of Dementia Research, New Frontiers. Alzheimer's Disease International, 2018, 1–48.
- P. Mendiola-Precoma, L.C. Berumen, K. Padilla, G. Garcia-Alcocer, Therapies for Prevention and Treatment of Alzheimer's Disease, *Biomed. Res. Int.* 2589276 (2016).
- J. Haam, J. L. Yakel, Cholinergic modulation of the hippocampal region and memory function, *J. Neurochem. (Suppl 2)*, 2017, 142, 111–121.
- P. Meena, V. Nemaish, M. Khatri, A. Manral, P.M. Luthra, M. Tiwari, Synthesis, biological evaluation and molecular docking study of novel piperidine and piperazine derivatives as multi-targeted agents to treat Alzheimer's disease, *Bioorg. Med. Chem.* 23 (5) (2015) 1135–1148.
- D. Galimberti, E. Scarpini, Old and new acetylcholinesterase inhibitors for Alzheimer's disease, *Expert Opin. Investig. Drugs* 25 (10) (2016) 1181–1187.
- X. Chen, L. Fang, J. Liu, C.G. Zhan, Reaction pathway and free energy profiles for butyrylcholinesterase-catalyzed hydrolysis of acetylthiocholine, *Biochemistry* 51 (6) (2012) 1297–1305.
- D. Torrero, Acetylcholinesterase inhibitors as disease-modifying therapies for Alzheimer's disease, *Curr. Med. Chem.* 15 (24) (2008) 2433–2455.
- A. Xu, F. He, X. Zhang, X. Li, Y. Ran, C. Wei, C. James Chou, R. Zhang, J. Wu, Tacrine-hydroxamate derivatives as multitarget-directed ligands for the treatment of Alzheimer's disease: Design, synthesis, and biological evaluation, *Bioorg. Chem.* 98 (2020), 103721.
- M. Atanasova, I. Dimitrov, S. Ivanov, Molecular Dynamics Simulations of Acetylcholinesterase–Beta-Amyloid Peptide Complex, *Cybernetics, and Information Technologies*, *Bulgarian Acad. Sci.* 20 (6) (2020) 140–154, <https://doi.org/10.2478/cait-2020-0068>.
- M.L. Bolognesi, A. Minarini, M. Rosini, V. Tumi atti, C. Melchiorre, From Dual Binding Site Acetylcholinesterase Inhibitors to Multi-Target-Directed Ligands (MTDLs): A Step Forward in the Treatment of Alzheimer's Disease, *Mini-Rev. Med. Chem.* 8 (10) (2008) 960–967.
- E. Viayna, T. Gómez, C. Galdeano, L. Ramfrez, M. Ratia, A. Badia, M.V. Clos, E. Verdager, F. Junyent, A. Camins, M. Pallàs, M. Bartolini, F. Mancini, V. Andrisano, M.P. Arce, M.I. Rodríguez-Franco, A. Bidon-Chanal, F.J. Luque, P. Camps, D. Muñoz-Torrero, Novel huprine derivatives with inhibitory activity toward β -amyloid aggregation and formation as disease-modifying anti-Alzheimer drug candidates, *Chem. Med. Chem.* 5 (11) (2010) 1855–1870.
- R.R. Ramsay, M.R. Popovic-Nikolic, K. Nikolic, E. Uliassi, M.L. Bolognesi, A perspective on multi-target drug discovery and design for complex diseases, *Clin. Transl. Med.* 7 (1) (2018) 3.
- G.V.M.S. Parmar, M.F. Khan, W. Akhtar, S.R. Haiderb, M. Alama, R. Khatoun, M. Akhter, T. Anwer, Ensuing New Derivatives in Developing Therapeutics for Alzheimer's Disease - A Review, *Int. J. Pharm. Sci. Rev. Res.* 45 (1) (2017) 113–125.
- Z. Luo, J. Sheng, Y. Sun, C. Lu, J.A. Yan, H.-B. Liu, L. Luo, X. Li Huang, Synthesis and Evaluation of Multi-Target-Directed Ligands against Alzheimer's Disease Based on the Fusion of Donepezil and Ebselen, *J. Med. Chem.* 56 (22) (2013) 9089–9099.
- M. Pudlo, V. Luzet, L. Ismaïli, I. Tomassoli, A. Iutzeler, B. Refouvet, Quinolone-benzylpiperidine derivatives as novel acetylcholinesterase inhibitor and antioxidant hybrids for Alzheimer disease, *Bioorg. Med. Chem.* 22 (8) (2014) 2496–2507.
- H.M. Greenblatt, C. Guillou, D. Guénard, A. Argaman, S. Botti, B. Badet, C. Thal, I. Silman, J.L. Sussman, The Complex of a Bivalent Derivative of Galanthamine with Torpedo Acetylcholinesterase Displays Drastic Deformation of the Active-Site Gorge: Implications for Structure-Based Drug Design, *J. Am. Chem. Soc.* 126 (47) (2004) 15405–15411.
- L. Fang, B. Kraus, J. Lehmann, J. Heilmann, Y. Zhang, M. Decker, Design and synthesis of tacrine-ferulic acid hybrids as multi-potent anti-Alzheimer drug candidates, *Bioorg. Med. Chem. Lett.* 18 (9) (2008) 2905–2909.
- S. Naz, L.T. Al-Kury, H. Nadeem, F.A. Shah, A. Ullah, R.Z. Paracha, M. Imran, S. Li, Synthesis, In Silico and Pharmacological Evaluation of New Thiazolidine-4-Carboxylic Acid Derivatives Against Ethanol-Induced Neurodegeneration and Memory Impairment, *J.-Inflamm. Res.* 15 (2022) 3643–3660.
- R.J. Obaid, E.U. Mughal, N. Naeem, M.M. Al-Rooqi, A. Sadiq, R.S. Jassas, Z. Moussa, Saleh A. Ahmed, Pharmacological Significance of Nitrogen-Containing Five and Six-Membered Heterocyclic Scaffolds as Potent Cholinesterase Inhibitors for Drug Discovery, *Process Biochem.* 120 (2022) 250–259.
- R.J. Obaid, N. Naeem, E.U. Mughal, M.M. Al-Rooqi, A. Sadiq, R.S. Jassas, Z. Moussa, Saleh A. Ahmed, Inhibitory Potential of Nitrogen, Oxygen and Sulfur-Containing Heterocyclic Scaffolds against Acetylcholinesterase and Butyrylcholinesterase, *RSC Adv.* 12 (31) (2022) 19764–19855.
- Ş. Demirayak, Z. Şahin, M. Ertaş, E.F. Bülbül, C. Bender, S.N. Bıltekin, B. Berk, B. N. Sağlık, S. Levent, L. Yurttas, Novel thiazole-piperazine derivatives as potential cholinesterase inhibitors, *J. Het. Chem.* 56 (12) (2019) 3370–3386.
- M. Shidore, J. Machhi, K. Shingala, P. Murumkar, M.K. Sharma, N. Agrawal, A. Tripathi, Z. Parikh, P. Pillai, M.R. Yadav, Benzylpiperidine-Linked Diarylthiazoles as Potential Anti-Alzheimer's Agents: Synthesis and Biological Evaluation, *J. Med. Chem.* 59 (12) (2016) 5823–5846.
- A. Kamal, A.B. Shaik, G.N. Reddy, C.G. Kumar, J. Joseph, G.B. Kumar, U. Purushotham, G.N. Sastry, Synthesis, biological evaluation, and molecular modeling of (E)-2-aryl-5-styryl-1,3,4-oxadiazole derivatives as acetylcholine esterase inhibitors, *Med. Chem. Res.* 23 (2014) 2080–2092, <https://doi.org/10.1007/s00044-013-0786-y>.
- J. Luo, Y.-M. Li, Turning the tide on Alzheimer's disease: modulation of γ -secretase, *Cell Biosci.* 12 (1) (2022) 2, <https://doi.org/10.1186/s13578-021-00738-7>.
- S. Das, V.K. Das, L. Saikia, A.J. Thakur, Environment-friendly and solvent-free synthesis of symmetrical bis-imines under microwave irradiation, *Green Chem. Lett. Rev.* 5 (3) (2012) 457–474.
- C. Napolitano, M. Borriello, F. Cardullo, D. Donati, A. Paio, S. Manfredini, Rapid Access to 1-Benzyl 2-Substituted Piperazines: Application to the Synthesis of 1-Benzyl-2-difluoro-methyl-Piperazine, *Synth. Comm.* 41 (14) (2011) 2031–2035.
- C. Yamali, H.L. Gul, A. Ece, P. Taslimi, I. Gulcin, Synthesis, molecular modeling, and biological evaluation of 4-[5-aryl-3-(thiophen-2-yl)-4,5-dihydro-1H-pyrazol-1-yl] benzenesulfonamides toward acetylcholinesterase, carbonic anhydrase I and II enzymes, *Chem. Biol. Drug Des.* 91 (2018) 854–866, <https://doi.org/10.1111/cbdd.13149>.
- S. Burmaoglu, A.O. Yilmaz, P. Taslimi, O. Algul, D. Kilic, I. Gulcin, Synthesis and biological evaluation of phloroglucinol derivatives having alpha-glycosidase, acetylcholinesterase, butyrylcholinesterase, carbonic anhydrase inhibitory activity, *Arch. Pharm.* 351 (2018) 1–12, <https://doi.org/10.1002/ardp.201700314>.
- R.Z. Cer, U. Mudunuri, R. Stephens, F.J. Lebeda, IC₅₀-to-Ki: a web-based tool for converting IC₅₀ to Ki values for inhibitors of enzyme activity and ligand binding, *Nucleic Acids Res.* 37 (2009) W441–W445.
- X. Li, H. Wang, Z. Lu, X. Zheng, W. Ni, J. Zhu, Y. Fu, F. Lian, N. Zhang, J. Li, H. Zhang, F. Mao, Development of Multifunctional Pyrimidine thiourea Derivatives as Potential Anti-Alzheimer Agents, *J. Med. Chem.* 59 (18) (2016) 8326–8344.
- K. Dam, M. Fichtemeier, T.D. Farr, P. Boehm-Sturm, M. Foddus, U. Dirnagl, O. Malysheva, M.A. Caudill, N.M. Jadavji, Increased homocysteine levels impair reference memory and reduce cortical levels of acetylcholine in a mouse model of vascular cognitive impairment, *Behav. Brain Res.* 321 (2017) 201–208.
- M. Attaroshan, O. Firuzi, A. Iraj, Sh. Sharifi, M. Tavakkoli, M. Vesal, M. Khoshneviszadeh, S. Pirhadi, N. Edraki, Imino-2H-chromene based derivatives as potential anti-alzheimer's agents: Design, synthesis, biological evaluation and in silico study, *Chem. Biodivers.* 19 (2022), e202100599.
- G.F. Makhaeva, S.V. Lushchekina, N.V. Kovaleva, T.Y. Astakhova, N.P. Boltneva, E. V. Rudakova, O.G. Serebryakova, A.N. Proshin, I.V. Serkov, T.P. Trofimova, V. A. Tafeenko, E.V. Radchenko, V.A. Palyulin, V.P. Fisenko, J. Kořaběčný, O. Soukup, R.J. Richardson, Amiridine-piperazine hybrids as cholinesterase inhibitors and potential multitarget agents for Alzheimer's disease treatment, *Bioorg. Chem.* 112 (104974) (2021), <https://doi.org/10.1016/j.bioorg.2021.104974>.
- G.F. Makhaeva, N.V. Kovaleva, E.V. Rudakova, N.P. Boltneva, S.V. Lushchekina, T. Y. Astakhova, E.N. Timokhina, O.G. Serebryakova, A.V. Shchepochkin, M. A. Averkov, I.A. Utepova, N.S. Demina, E.V. Radchenko, V.A. Palyulin, V. P. Fisenko, S.O. Bachurin, O.N. Chupakhin, V.N. Charushin, R.J. Richardson, Derivatives of 9-phosphorylated acridine as butyrylcholinesterase inhibitors with antioxidant activity and the ability to inhibit β -amyloid self-aggregation: potential therapeutic agents for Alzheimer's disease, *Front. Pharmacol.* 14 (2023) 1219980, <https://doi.org/10.3389/fphar.2023.1219980>.

- [35] J. Cheung, M.J. Rudolph, F. Burshteyn, M.S. Cassidy, E.N. Gary, J. Love, M. C. Franklin, J.J. Height, Structures of human acetylcholinesterase in complex with pharmacologically important ligands, *J. Med. Chem.* 55 (22) (2012) 10282–10286.
- [36] O. Gerlits, K.Y. Ho, X. Cheng, D. Blumenthal, P. Taylor, A. Kovalevsky, Z. Radić, A new crystal form of human acetylcholinesterase for exploratory room-temperature crystallography studies, *Chem. Biol. Interact.* 309 (2019), 108698.
- [37] F. Nachon, E. Carletti, C. Ronco, M. Trovaslet, Y. Nicolet, L. Jean, P.Y. Renard, Crystal structures of human cholinesterases in complex with huprine W and tacrine: elements of specificity for anti-Alzheimer's drugs targeting acetyl- and butyrylcholinesterase, *Biochem. J.* 453 (3) (2013) 393–399.
- [38] J. Wiesner, Z. Kriz, K. Kuca, D. Jun, J. Koca, Acetylcholinesterases – the structural similarities and differences, *J. Enzyme Inhib. Med. Chem.* 22 (4) (2007) 417–424, <https://doi.org/10.1080/14756360701421294>.
- [39] P. Masson, E. Carletti, F. Nachon, Structure, activities, and biomedical applications of human butyrylcholinesterase, *Protein Peptide Lett.* 16 (2009) 1215–1224.
- [40] B.K. Shoichet, S.L. McGovern, B. Wei, J.J. Irwin, Lead discovery using molecular Docking, *Curr. Opin. Chem. Biol.* 6 (4) (2002) 439–446.
- [41] J.C. Phillips, D.J. Hardy, J.D.C. Maia, J.E. Stone, J.V. Ribeiro, R.C. Bernardi, R. Buch, G. Fiorin, J. Henin, W. Jiang, R. McGreevy, M.C.R. Melo, B.K. Radak, R. D. Skeel, A. Singh aroy, Y. Wang, B. Roux, A. Aksimentiev, Z. Luthey-Schulten, L. V. Kale, K. Schulten, C. Chipot, E. Tajkhorshid, Scalable molecular dynamics on CPU and GPU architectures with NAMD, *J. Chem. Phys.* 153 (4) (2020), 044130, <https://doi.org/10.1063/5.0014475>.
- [42] J.V. Ribeiro, R.C. Bernardi, T. Rudack, K. Schulten, E. Tajkhorshid, QwikMD-Gateway for Easy Simulation with VMD and NAMD, *Biophys. J.* 114 (3) (2018) 673a–a674.
- [43] K. Vanommeslaeghe, E. Hatcher, C. Acharya, S. Kundu, S. Zhong, J. Shim, E. Darian, O. Guvench, P. Lopes, I. Vorobyov, A.D. Mackerell Jr., CHARMM general force field: A force field for drug-like molecules compatible with the CHARMM all-atom additive biological force fields, *J. Comput. Chem.* 31 (4) (2010) 671–690, <https://doi.org/10.1002/jcc.21367>.
- [44] B.R. Miller III, T.D. McGee Jr, J.M. Swails, N.H. Homeyer, A.E. Roitberg, MMPBSA, Py: an efficient program for end-state free energy calculations, *J. Chem. Theory and Compute.* 8 (2012) 3314–3321.
- [45] F.J. Luque, J.M. Lopez, M. Orozco, *Theor. Chem. Acc.* 103 (2000) 343–345.
- [46] I. Kılıç Cıkla, S. Güvelci, M. Yavuz, T. Bal Demirci, B. Ülk üseven, 5-Methyl-2-acetophenone-thiosemicarbazone and its nickel (II) complex: Crystallographic, spectroscopic (IR, NMR and UV) and DFT studies, *Polyhedron* 105 (2016) 104–114.
- [47] C.A. Lipinski, F. Lombardo, B.W. Dominy, P.J. Feeney, *Adv. Drug Deliv. Rev.* 46 (2001) 3–26.
- [48] D.F. Veber, S.R. Johnson, H.Y. Cheng, B.R. Smith, K.W. Ward, K.D. Kopple, *J. Med. Chem.* 45 (2002) 2615–2623.
- [49] A. Jarrahpour, J. Fathi, M. Mimouni, T. Ben Hadda, J. Sheik, Z.H. Chohan, A. Parvez, *Med. Chem. Res.* 21 (2012) 1984–1990.
- [50] A. Parvez, M. Jyotsna, M.H. Youssoufi, T. Ben Hadda, *Phosphorus Sulfur Silicon Relat. Elem.* 7 (2010) 1500–1510.
- [51] A. Parvez, J. Meshram, V. Tiwari, J. Sheik, R. Dongre, M.H. Youssoufi, T. Ben Hadda, *Eur. J. Med. Chem.* (2010,45,) 4370–4378.
- [52] P. Ertl, B. Rohde, P. Selzer, *J. Med. Chem.* 43 (2000) 3714–3717.
- [53] Mayuri Gupta, Hyeok Jun Lee, Christopher J. Barden, and Donald F. Weave, The Blood–Brain Barrier (BBB) Score, *J. Med. Chem.* 2019, 62, 21, 9824–9836. doi. org/ 10. 1021/ acs.jmedchem.9b01220.
- [54] T. Földesi, G. Sipos, R. Adamik, B. Nagy, B.L. Tóth, A. Bényei, K.J. Szekeres, G. G. Láng, A. Demeter, T.J. Peelen, Z. Novák, Design and application of diimine-based copper (I) complexes in photoredox catalysis, *Org. Biomol. Chem.* 17 (36) (2019) 8343–8347.
- [55] M.S.Y. Khan, G. Chawla, Tetrahydroimidazoles - A promising group of expected NSAIDs - Their synthesis and anti-inflammatory activity, *Ind. J. Chem. - Section B Org. Med. Chem.* 41 (2002) 653–663.
- [56] V. Sharma, M.S.Y. Khan, Synthesis of novel tetrahydroimidazole derivatives and studies for their biological properties, *Eur. J. Med. Chem.* 36 (7) (2001) 651–658.
- [57] S.M. Kishk, K.J. McLean, S.M.A. Sood, M.S. Helal, I. Gomaa, S.M. Salama, L. P. Mostafa, S. de Carvalho, A.W. Munro, C. Simons, Synthesis and biological evaluation of novel cYY Analogs targeting *Mycobacterium tuberculosis* CYP121A1, *Bioorg. Med. Chem.* 27 (8) (2019) 1546–1561.
- [58] T.A. Sidorova, A.G. Nigmatov, E.S. Kakpakova, A.A. Stavrovskaya, G. K. Gerassimova, A.A. Shtil, E.P. Serebryakov, Effects of Isoprenoid analogs of SDB-Ethylenediamine on Multidrug Resistant Tumor Cells Alone and in Combination with Chemotherapeutic Drugs, *J. Med. Chem.* 45 (24) (2002) 5330–5339.
- [59] H.A.A.A. El-wahab, M. Accietto, L.B. Marino, K.J. McLean, C.W. Levy, H.M. Abdel-Rahman, M.A. El-Genidy, A.W. Munro, A.S. Aboraia, C. Simons, Design, synthesis and evaluation against *Mycobacterium tuberculosis* of azole piperazine derivatives as dicycetyrosine (cT) mimics, *Bioorg. Med. Chem.* 26 (1) (2018) 161–176.